IET Renewable Power Generation

Special Issue Call for Papers

Be Seen. Be Cited.
Submit your work to a new IET special issue

Connect with researchers and experts in your field and share knowledge.

Be part of the latest research trends, faster.

Read more

The Institution of Engineering and Technology

Received: 23 April 2022 | Revised: 16 September 2022 | Accepted: 19 September 2022

DOI: 10.1049/rpg2.12611

IET Renewable Power Generation

The Institution of Engineering and Technology WILEY

ORIGINAL RESEARCH

Reliability evaluation of the renewable energy-based microgrids considering resource variation

Ayoub Nargeszar[1] | Amir Ghaedi[2] | Mehdi Nafar[1] | Mohsen Simab[1]

[1]Islamic Azad University, Marvdasht Branch, Marvdasht, Iran

[2]Islamic Azad University, Dariun Branch, Iran

Correspondence
Amir Ghaedi, Islamic Azad University, Dariun Branch, Iran.
Email: amir.ghaedi@miau.ac.ir

Abstract

A suitable mixture of renewable resources including wind, tidal and photovoltaic units can be used in the microgrids installed in coastal areas or islands. However, the variation in the renewable resources such as wind speed, tidal current speed and solar radiation is significant that affects the reliability performance of these microgrids. Thus, to accurately evaluate the reliability of the microgrids, the failure rate of composed components affected by the variation in the renewable resources must be considered. To study the impact of variation in the temperature and renewable resources on the failure rate of components, different equations including Arrhenius law, temperature modification factor, fatigue strength, bending and contact stress, limit state function of turbine, thermal loss of semiconductor devices, the temperature rise of transformer and cable, the temperature coefficient of voltage and power of photovoltaic panels are developed. According to the developed equations, the components failure rate, and consequently the failure rate of the microgrid considering the variation in the temperature and renewable resources are determined. Then, by simulation, the impact of different energy sources on the failure rate of the whole system is evaluated and the reliability in a microgrid consisting of offshore renewable energy sources will be studied.

1 | INTRODUCTION

In recent years, the renewable energy-based generation units such as wind turbines, photovoltaic (PV) panels, current type tidal units and wave energy conversion systems are increasingly used to supply the local loads in the microgrids. In addition to benefits such as reducing voltage drops, reducing power losses, increasing the reliability and improving the voltage profile, the microgrids allow the renewable energy-based resources to be used to supply the local consumers. However, attributable to dissimilarity in the renewable resources, the power produced by the renewable energy-based generation units varies widely in time that affects different aspects of these microgrids that must be studied. Due to the importance of microgrid reliability, many of the past researches have been devoted to this topic. In [1], mission-profile-based reliability assessment of DC microgrids in system-level is performed. In this research, to study the reliability of the power electronics components and systems such as capacitors and power semiconductors used in the microgrids, the climate variation and operating limitations are considered in the microgrid, which also includes the configuration of the converters, the available energy sources and the interconnected structure of the system. The presented approach is examined on a DC microgrid, including PV panel, fuel cell and battery to calculate the unreliability of these generation units considering the years of the operation. However, to calculate the failure rate of the understudied generation units the effect of other affective components are not considered and the failure rate of equipment and elements used in the system is not taken into account due to the diversity of renewable energy sources. Besides, only PV system as a renewable resource is considered in the DC microgrid. In [2], reliability assessment of the stand-alone microgrids including PV generation units, microturbines, comprehensive loads and energy storage systems is achieved. In this research, in order to model the output power of PV arrays, the beta probability density function has been used. Several reliability indicators are discussed below, including loss of load probability, average service availability index, system

average interruption duration index, system average interruption frequency index and customer average interruption duration index considering PV penetration, which are calculated using the Monte Carlo method. However, several disadvantages of this paper are excluded as the composed components failure rate ignoring and the solar radiation variation effects on the reliability indices of the PV-based microgrids. In [3], reliability evaluation of an isolated microgrid including wind turbine, PV system, distributed generation units consuming fuel and the loads with capability to contribute in load-frequency control (LFC) is performed. In this literature, the impact of the random failures of cyber-physical system including switches, circuit breakers, microsource controllers, current transformers and potential transformers resulted in the malfunction of the frequency control on the reliability indices is investigated using of the Monte Carlo simulation method. However, in the proposed reliability assessment technique, the impact of affective components such as generators, PV panels and transformer is not considered. In [4], short-term reliability evaluation of the islanded microgrids using of the time-varying probability ordered tree screening algorithm is performed and the reliability indices of the understudied microgrid containing loss of load probability and expected energy not supplied (EENS) are determined. This paper calculates, based on the proposed algorithm, the reliability indices of the islanded microgrid including microturbines, wind turbines, PV systems, energy storage systems and loads. However, in the proposed reliability assessment method, the impact of the variation in the renewable resources and the components failure rate are not taken into account. In [5], a novel sequential sampling algorithm is proposed to evaluate the reliability of the microgrids including microturbines and PV systems. This paper uses the variation method to determine the optimal probability density function of the random variables. However, the variable rate of failure for PV system dependent on the solar irradiation power is not considered. In [6], the superconducting magnetic energy storage system is used to smooth the fluctuated power of the PV panel and consequently, enhance the reliability of the microgrids containing PV generators. In this research, a fuzzy logic approach is projected in order to advance the reliability of the microgrids including PV systems and superconducting magnetic energy storage systems. However, the impact of variable renewable resource on the reliability indices and also the components failure rate is not considered in this study. In [7], to evaluate the reliability and economics of the microgrids in distribution systems, new metrics including reliability parameters for a microgrid in the islanded mode, indices indicating distributed generation and load characteristics in the microgrid, microgrid economic indices and customer-based reliability indices, are proposed. In this study, using two-step Monte Carlo simulation method, the reliability and economics of a microgrid containing intermittent generation units is determined. The drawback of this paper is that the effect of the changing in sunlight and wind speed on the reliability indices of the understudied microgrid containing wind turbine and PV system is not considered. In [8], to model the reliability performance of the microgrids in the hot standby mode, hybrid methods including Markov model, fault tree analysis, reduced binary decision diagram and reduced sequential binary decision diagram are proposed. To investigate the effectiveness of the proposed techniques, reliability analysis of the IEEE 5-bus microgrid system including 100 kW PV system and diesel generator is performed. However, the influence of the solar radiation changing continuously on the PV system failure rate is not done in the modelling. In [9], the optimal size of the energy storage system in the networked microgrid considering the reliability and resilience indices is determined. This paper develops a bi-level optimization model for the energy storage sizing problem. In the upper-level problem, the annual profit is maximized, and in the lower-level problem, the profit under multiple operating scenarios is maximized. However, the changing in solar radiation cause the variable failure rate in the microgrid-based PV systems, which is not molded in the proposed framework. In [10], the models of the momentary event are developed to be integrated in the reliability evaluation of the active distribution systems. This paper proposes a novel aggregared reliability even model to consider the effect of the random failures of the distribution systems including voltage sags, momentary interruptions and sustained interruptions on the reliability indices of distribution systems. However, the failure rate of the generation units of the distribution system is not considered in the proposed study. In [11], a hierarchical structure is proposed to assess the reliability of an islanded hybrid microgrid. This paper models the reliability performance of the power converters used in the renewable energy-based generation units considering the power semiconductors arrangement and loading condition. However, since changes in weather conditions affect PV output power and network reliability indicators, they are not discussed in this paper. In [12], a novel reliability assessment method based on the time correlation model is introduced to evaluate the reliability of the microgrids. This paper develops the model of the microgrid, based on the distributed power supply output model, load and component fault model, and then using of the improved Latin Hypercube sampling method, the generated power of the wind turbine and PV system is sampled. However, since the failure rate of turbines and other renewable sources is not modelled in this paper, it can be omitted as a complete framework. In [13], reliability assessment of the microgrids considering the distributed energy storage systems is performed. This paper solves, using of the dynamic programming, the unit commitment problem of the microgrid in two cases equipped to the energy storage system and without energy storage system. Nevertheless, the disadvantages of this paper include not considering variation in the renewable resources.

In [14], the Markov chain model is proposed to study the reliability performance of the centralized and decentralized microgrids. In [15], a stand-alone microgrid including the PV systems, diesel generator and battery is considered and using the mixed integer linear programming approach, the optimal size of the associated units is determined. This paper uses the rolling horizon-based Sequential Monte Carlo method for reliability evaluation of the microgrid to determine the optimal size of the

units. In [16], the failure rate of the power electronic converters used in the generation units of the microgrids is proposed to be non-exponential, and based on this fact, the reliability assessment of the microgrids is performed. In [17], to analyse the overall reliability of an islanded microgrid containing high penetration level of the renewable resources, the impact of the operation failure probability of power electronic components is considered. This paper uses the hybrid energy storage system instead of the conventional battery storage system to improve the reliability of the microgrid. In [18], the impact of the distributed energy resources, electrical vehicles and energy storage system on the reliability, power quality, energy management and control strategies of the microgrids is studied.

This paper considers a suitable mixture of renewable resources including wind unit, tidal turbine and PV system to be installed in a coastal or island microgrid. To determine the reliability performance of these microgrids, the impact of composed components failure on the overall failure of microgrid must be studied. Besides, due to the variation in the renewable resources and ambient temperature, for accurate reliability calculation, it is necessary to determine the impact of variation in wind speed, tidal current speed, solar radiation and temperature on the failure rate of composed components. Thus, the innovations of this paper are:

- Detailed reliability model of a renewable energy-based microgrid containing wind, tidal and PV systems is developed, and the impact of failure of all effective composed components on the overall failure of microgrid is considered.
- Due to the variation in the renewable resources and temperature, the impact of all effective parameters including wind speed, tidal current speed, solar radiation and temperature on the failure rate of all components is studied. For this purpose, different equations including Arrhenius law, temperature modification factor of alloy steels, fatigue strength, bending and contact stress equations of mechanical parts, limit state function of turbine, thermal loss of semiconductor devices, the temperature rise of transformer and cable, the temperature coefficient of voltage and power of PV panels are developed.
- The technology associated to the generator used in the wind and tidal units affects the reliability performance of these units. For comprehensive study of these units, two well-known technologies including permanent magnet synchronous generator (PMSG) and double fed induction generator (DFIG) are considered.

Based on the goals of this paper, it is organized as follow: the structure of the understudied microgrids and the included modules of the power generation units with renewable energy technology are introduced in Section 2. The failure rate of the elements used in the system based on temperature changes is described in Section 3. Section 4 is devoted on the implementation of the proposed method in practice and reliability evaluation approach is introduced. Simulation results are given in Section 5 and the conclusion is presented to summarize the findings in Section 6.

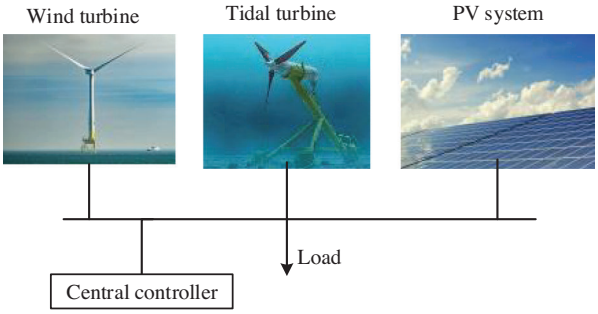

FIGURE 1 The structure of the renewable energy-based microgrid

2 | THE STRUCTURE OF THE RENEWABLE ENERGY-BASED MICROGRID

The structure of a renewable energy-based microgrid containing the wind turbines, tidal units and PV systems to supply the required load is shown in Figure 1. To control and manage the generated power of the renewable resources of the microgrid, a central control system that plays a major role in smooth stable operation of the microgrid is taken into account. In the renewable energy-based system, the central controller performs the same function that the supervisory control and data acquisition (SCADA) does in the power system.

The composed components of a typical wind turbine are shown in Figure 2. To extract the kinetic energy of the moving air mass, a wind generation unit is equipped to the wind turbine, gearbox for change the rotation speed, generator for electric power generation, electrical converters for voltage and frequency adjustment, control system for control the electrical converters, transformer for voltage matching and cable for power transmission [19]. Different generator technologies are used in the wind generation units including squirrel cage induction generators, PMSG, electrically excited synchronous generators and DFIG [20].

The basis of electricity generation in wind units and current type tidal plants are similar. Thus, the structure of the tidal generation units would be the same of the wind power plants structure [21]. Due to the high potential of tidal currents and the maturity of technologies associated to marine current turbine, numerous tidal current farms such as 10 MW Anglesey tidal farm in Wales, 10 MW Sound of Islay tidal farm in Scotland and 12 MW Raz Blanchard tidal farm are constructed and operated in past years [21]. Two types of ocean energies including wave and tidal current are most advanced and are expected to use for electric power generation in future [22]. In [22], a review of the current states of these renewable resources is performed and different aspects of these energies including environmental impacts, life cycle, social impacts, cost–benefit analysis, grid integration, resource variability, power quality and control, installation, operation and maintenance are discussed. From resource variability point of view, the tidal current energy is periodic, and so, the forecasting of this

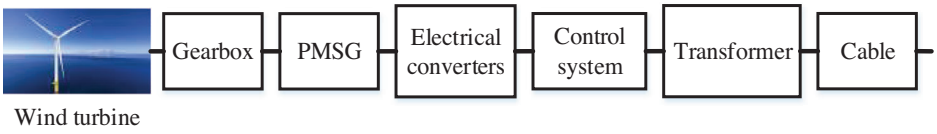

FIGURE 2 The constitutive components of a typical wind power generation unit

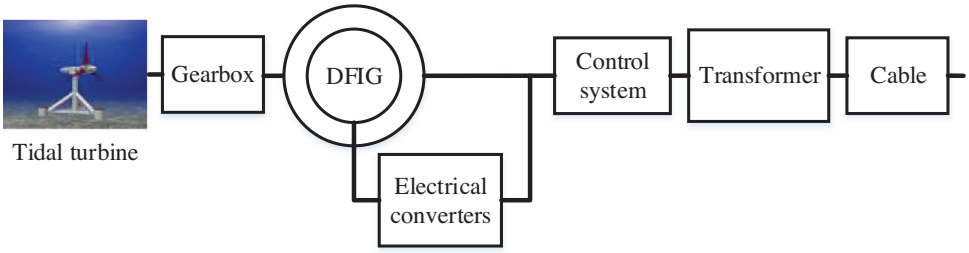

FIGURE 3 The composed components of a typical tidal turbine

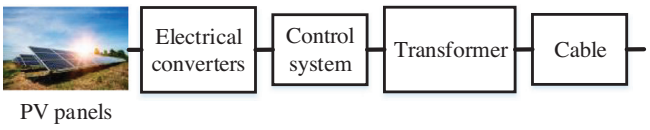

FIGURE 4 The composed components of a typical PV system

energy over long time horizons with high accuracy is possible. However, the wave energy is a stochastic resource and so, accurate forecasting of this resource is difficult [22]. Thus, due to the predictability of tidal currents, the tidal turbines are considered to be installed in the renewable energy-based microgrid.

Among different generator technologies used in the wind and tidal turbines to convert the kinetic energy of the wind speed and tidal current streams, DFIG and PMSG are widely have been used, in recent years [23]. Thus, to investigate both technologies, the understudied wind and tidal turbines are, respectively, based on the PMSG and DFIG technologies. In Figure 3, the composed components of a tidal power generation unit equipped to the DFIG expertise, including tidal turbine, gearbox, DFIG, electrical converters, control system, transformer and cable are presented.

In a typical PV system, the energy of the sunlight is directly converted to the DC electric power using of the p-n junctions of the PV cells. To transfer the DC generated power of the PV panels, the electrical converters for maximum power point tracking (MPPT) and converting the DC voltage to the AC voltage, control system for control the electrical converters, transformer for voltage matching and cable for power transmission are used [24]. The composed components of a typical PV system are presented in Figure 4.

3 | THE FAILURE RATE OF RENEWABLE ENERGY-BASED GENERATION UNITS

In this part of the paper, the failure rate of wind generation units, tidal turbines and PV systems according to the composed components failure rate considering the effect of the variation in the renewable resources including wind turbine speed, solar radiation and tidal current speed and furthermore, the temperature variation is derived. For each component, a two-state Markov model including up and down states, as presented in Figure 5, are considered. The failure rate (λ) is the transition rate from up state to the down state, and the repair rate (μ) is the transition rate from down state to the up state [25].

The probability of the Markov model up and down states presented in Figure 5 can be calculated as (1) [25].

$$P_{up} = \frac{\mu}{\lambda + \mu}, \quad P_{down} = \frac{\lambda}{\lambda + \mu}. \tag{1}$$

3.1 | The failure rate of wind turbine

In this part, the equivalent failure rate of a wind turbine based on the PMSG technology is determined. As can be shown in

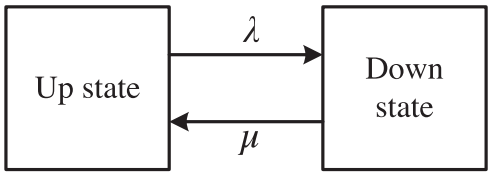

FIGURE 5 The two-step Markov model for the system components

Figure 2, the failure of the main components of a wind generation unit covering gearbox, PMSG, electrical converters, control system, transformer and cable leads the transmission of the produced power of the wind turbine to the microgrid stops and the output power would be zero. Thus, according to the reliability concept, since all of this equipment is located in series in the system, the equivalent failure rate of the wind generation unit and repair rate can be calculated as [25]:

$$\lambda_t = \sum_{k=1}^{n} \lambda_k, \tag{2}$$

$$\mu_t = \frac{\lambda_t}{\sum_{k=1}^{n} \frac{\lambda_k}{\mu_k}}, \tag{3}$$

where λ_t and μ_t are, respectively, equivalent failure rate and repair rate of the wind turbine composed of n series components in the reliability model. In (3), λ_k and μ_k are failure rate and repair rate of main elements of the wind turbine structure, respectively. In this phase, the effect of temperature and wind speed on the failure rate of wind energy system will be calculated. In [26–29], the gearbox reliability concepts used in the some types of wind turbines including spur, helical and cylindrical gears considering the effect of the pitting and tooth root breakage, bending and contact fatigue, fretting corrosion and plastic deformation is studied. The permissible bending and contact stresses of the gearbox can be calculated as [26–29]:

$$\sigma_F = \frac{\sigma_{F\lim} Y_N}{S_F Y_\theta Y_Z}, \tag{4}$$

$$\sigma_H = \frac{\sigma_{F\lim} Z_N Z_W}{S_H Y_\theta Y_Z}, \tag{5}$$

where σ_F, σ_H, σ_{Flim}, σ_{Hlim}, Y_N, S_F, Y_Z, Z_N, Z_W, S_H and Y_θ are permissible bending stress, permissible contact stress, fatigue limit for bending stress, fatigue limit for contact stress, stress cycle factor for bending strength, safety factor for bending stress, reliability factor, stress cycle factor for pitting resistance, hardness ratio factor for pitting resistance, safety factor for pitting and temperature factor. The hours of expected fatigue lifetime considering the rotational speed of the gearbox can be determined as [26–29]:

$$H_{\sigma H} = \frac{n_{Lh}}{60nq}, \tag{6}$$

$$H_{\sigma F} = \frac{n_{Lf}}{60nq}, \tag{7}$$

where $H_{\sigma H}$, $H_{\sigma F}$, n_{Lh}, n, q and n_{Lf} are the expected fatigue lifetime considering contact stress and bending stress, number of load cycles expected by pitting, rotational speed (rpm), number of load application by one turn of gear and number of load cycles expected by fatigue feature. It is deduced from the reliability analysis of the gearbox performed in [26–29], the relationship between the probability of the failure of the gearbox and the rotational speed is linear. The rotational speed of the turbine, generator and gearbox is dependent on the wind speed as [20]:

$$n = \frac{60\omega}{2\pi} = \frac{60v}{2\pi r}, \tag{8}$$

where n is the rotational speed in rpm, ω is the angular velocity in rad/s, v is the wind speed and r is the radius of the rotational device. In the wind turbine, the temperature of the composed components does not exceed 100°C. The temperature modification factor associated to the carbon and alloy steels widely used in the gear manufacturing can be determined as [30]:

$$k_d = 0.975 + 0.000432T_F - 0.115 \times 10^{-5} T_F^2 + 0.104 \times 10^{-8} T_F^3 - 0.595 \times 10^{-12} T_F^4, \tag{9}$$

where T_F is the temperature of the device in Fahrenheit and is between 70 and 1000°F. The fatigue strength of the gearbox components is inversely proportional to the endurance limit that is determined as [30]:

$$S_e = k_a k_b k_c k_e k_f S_e', \tag{10}$$

where S_e and S_e' are endurance limit and base endurance limit, k_a, k_b, k_c, k_d, k_e, k_f are the modification coefficients associated to the surface condition, size, load, temperature, reliability and miscellaneous-effects. Thus the failure of the gearbox components can be determined as [30]:

$$\lambda_{gearbox}(T_F) = \frac{k_d(T_F)}{k_d(T_{F0})} \lambda_{gearbox}(T_{F0}). \tag{11}$$

In this stage, the failure rate of the wind turbine considering the variation in the wind speed and ambient temperature is determined. The probability of down state of a wind turbine arisen from failure of the rotor blades considering the wind speed can be determined as [31]:

$$P_{down-state} = probability\ of\ [f(v) \le 0], \tag{12}$$

where $f(v)$ is the limit state function which can be mathematically obtained in (13) [31].

$$f(v) = f_c - \frac{C_m M_f}{Z_f}. \tag{13}$$

In (13), Z_f is the modulus of the spar section of the corresponding axis in m^3, M_f is the flap-wise bending moment corresponding to the blade root in kNm, f_c is the spar material strength in kN/m^2 and C_m is modelled to investigate the inherent uncertainty of the turbine failure. The flap-wise bending moment of the wind turbine considering the wind speed can be determined as [31]:

$$M_f = -45.9 + 52.3v. \tag{14}$$

To consider the uncertainty nature of the turbine failure, the normal distribution function is used for C_m which include the mean value as 1 and the standard deviation as 0.39 [31]. As mentioned the temperature of the wind turbine components

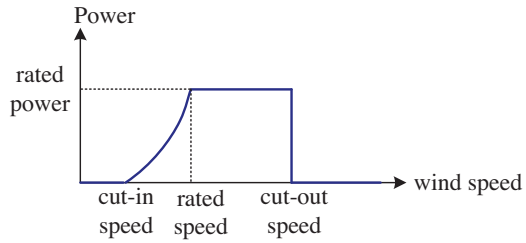

FIGURE 6 The power curve of the wind turbine

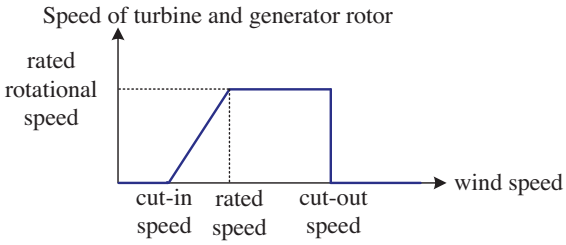

FIGURE 7 The rotor speed considering the wind speed

does not exceed 100°C. Equation (11) shows the failure rate of wind turbine in checking the reliability of the system along with the effect of ambient temperature. PMSG failure also depends on the failure rate of electrical and mechanical components. In [32–34], the temperature rise of the generators arisen from the current of the stator windings is calculated. According to the Arrhenius law, the failure rate of the generator at temperature θ in °C can be calculated as [35]:

$$\lambda(\theta) = \lambda(25^{\circ}\mathrm{C})e^{\frac{-E_a}{k}\left(\frac{1}{\theta+273}-\frac{1}{298}\right)}, \tag{15}$$

where $\lambda(25^{\circ}\mathrm{C})$ is the failure rate of the generator at 25°C, E_a is the activation energy and k is the Boltzmann constant. According to the PMSG wind turbine power generation curve shown in Figure 6, the effect of wind speed changes on the failure rate of electrical and mechanical components can be understood.

According to the wind turbine generator generating power diagram shown in Figure 6, the turbine output power will be zero for speeds less than the cut-in speed and more than cut-off speed. This feature is intended to prevent power loss and damage to components. Moreover, in the allowable wind speed range between cut-in and rated speed, the output power of the turbine is proportional to the third power of the wind speed. For wind speeds between nominal speed and cut-off speed, the output power is constant. The induced voltage in the stator windings of the generator is proportional to the magnetic flux of the permanent magnet and the rotational speed of the rotor. Thus, the rotor speed and induced voltage considering the wind speed would be as presented in Figures 7 and 8.

Since the current of stator windings is determined by dividing the turbine power by the stator voltage, so with the availability of wiring resistance, power losses can be equated (9) [20].

$$P_{loss\text{-}PMSG} = 3R_G I_G^2, \tag{16}$$

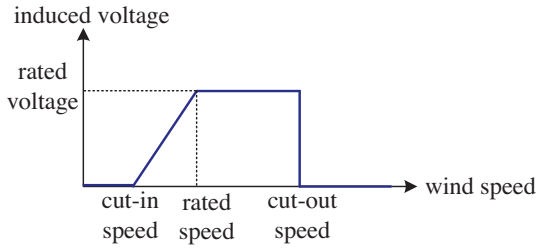

FIGURE 8 The induced voltage in the stator windings versus wind speed

where R_G and I_G are the stator winding resistance and the stator current, respectively. The temperature of the generator insulation can be determined as [20]:

$$T_G = T_a + R_{GH} P_{loss\text{-}PMSG}, \tag{17}$$

where T_a is the ambient temperature and R_{GH} is the equivalent thermal resistance of the windings to the generator body including different insulation materials. According to the Arrhenius law, the failure rate of the electrical part of the PMSG considering the variation in the wind speed and ambient temperature can be determined as (12). The failure rate of the generator due to the mechanical failures can be determined based on the fatigue stress of the rotational part, that is, rotor. The failure rate of the generator arisen from the mechanical failures is proportional to the rotational speed [26–30]. The temperature of the generator components does not exceed 100°C, and so, considering the effect of temperature on the failure rate of the components given in Equation (9), the total failure rate of PMSG can be determined as (15) [25].

$$\lambda_{PMSG} = \lambda_{PMSG-e} + \lambda_{PMSG-m}, \tag{18}$$

where $\lambda_{PMSG\text{-}e}$ and $\lambda_{PMSG\text{-}m}$ are failure rates of the PMSG arisen from the failures of the electrical and mechanical parts of the generator, respectively. The typical structure of the electrical converters used in the wind turbines based on the PMSG technology is presented in Figure 9. As observed in the aforementioned figure, a rectifier is connected to the stator of the PMSG to convert the AC voltage with variable frequency and magnitude to the DC voltage. A capacitor is also placed in the DC link to smooth the output voltage. Then, an inverter is connected to the DC link to convert the DC voltage to the AC voltage. To calculate the failure rate of the rectifier or inverter, the temperature of every semiconductor piece used in the converters must be determined as [36]:

$$T_{sd} = T_a + P_S R_{TH} + P_{sd} R_{CH}, \tag{19}$$

where T_{sd} is the temperature of each semiconductor device including diode, thyristor or insulated-gate bipolar transistor (IGBT) used in the rectifier or inverter, P_{sd} is the thermal loss of the associated semiconductor device, R_{TH} is the equivalent thermal resistance of interface case to the heat sink and R_{CH} is the thermal resistance from the semiconductor interface case to the associated junction. The rectifier includes six thyristors and six diodes, while the inverter includes six IGBTs and six

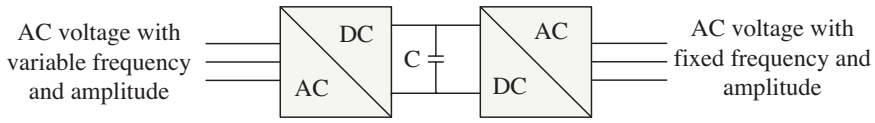

FIGURE 9 The structure of the electrical converters

diodes. Thus, P_S can be calculated as (17) and (18), for rectifier and inverter, respectively [36].

$$P_{S\text{-}rectifier} = 6 \times (P_{sd\text{-}thyristor} + P_{sd\text{-}diode}), \tag{20}$$

$$P_{S\text{-}inverter} = 6 \times (P_{sd\text{-}IGBT} + P_{sd\text{-}diode}). \tag{21}$$

The thermal loss of each semiconductor device including diode, thyristor or IGBT can be calculated as [36]:

$$P_{sd} = P_{sd\text{-}cond} + P_{sd\text{-}rec} = \frac{1}{2}\left[U_0\frac{I_P}{\pi} + r\frac{I_P^2}{4}\right] \pm m\cos\varphi\left[U_0\frac{I_P}{8} + r\frac{I_P^2}{3\pi}\right] + \frac{U_{DC}}{U_{nom}}P_{SW}, \tag{22}$$

where $P_{sd\text{-}cond}$, $P_{sd\text{-}rec}$, P_{SW} are the thermal losses of the diode, thyristor or IGBT associated to the conduction, recovery and switching states, respectively. The voltages U_0, U_{nom} and U_{DC} are voltage drop on the semiconductor device, reference voltage and DC link voltage, respectively. The parameter r is the resistance of the semiconductor device, m is the modulation index, ϕ is the angle between voltage and current and I_P is the peak value of the current passing through each phase of the rectifier or inverter that can be calculated as (20) and (21), respectively. The sign of the second term in (19) for the IGBTs in the inverter operation state is positive and in the rectifier operation state is negative, while, for the thyristors and diodes in the inverter operation state, the sign is negative and in the rectifier operation state is positive [36].

$$I_{P\text{-}rectifier} = \frac{\sqrt{2}P_G}{\sqrt{3}V_G}, \tag{23}$$

where P_G and V_G are the generated power and induced voltage of the PMSG that are calculated based on the power curve of the wind turbine (Figure 6) and the magnitude of the stator voltage (Figure 8) [25].

$$I_{P\text{-}inverter} = I_{P\text{-}rectifier}\frac{V_G}{V_i}, \tag{24}$$

where V_i is the output voltage of the inverter. The failure rate of every semiconductor piece in number of failures at 10^6 h considering the variation in the ambient temperature and wind speed those result in the variation in the temperature of the junction can be calculated as [36]:

$$\lambda = \lambda_1 k_1\pi_1 + \lambda_2 k_2\pi_2 + \lambda_3\pi_3 + \lambda_4, \tag{25}$$

where λ_1, λ_2 and λ_3 are the base failure rates of the conducting, non- conducting and temperature effect cycling contributions, λ_4 is the failure rate associated to the solder joint and electrical overstress contribution, k_1 and k_2 are the acceleration parameters associated to the conducting and non-conducting modes that can be calculated in (23) [36].

$$k_1 \text{ or } k_2 = e^{\frac{-E_a}{k}\left(\frac{1}{T_{sd}+273} - \frac{1}{298}\right)}. \tag{26}$$

However, the activation energy values for the operating and non-operating states of the semiconductor devices are different. The factors π_1 and π_2 are used to model the duty cycle for conducting and non-conducting modes which are determined in (24) and (25), respectively [36].

$$\pi_1 = \frac{1 - P_{non}}{DC_{op}}, \tag{27}$$

$$\pi_2 = \frac{P_{non}}{DC_{nonop}}, \tag{28}$$

where DC_{op} and DC_{nonop} are constant that is given for a specific semiconductor device, and P_{non} is the probability of the generator non-conducting mode. The coefficient π_3 is associated to the delta temperature cycling acceleration that can be determined as [36]:

$$\pi_3 = \left(\frac{T_{sd} - T_a}{DT}\right)^2, \tag{29}$$

where DT is a constant that is given for a specific semiconductor device. The failure rate of the electrical converters can be calculated as [25]:

$$\lambda_{ec} = \lambda_r + \lambda_c + \lambda_i, \tag{30}$$

where λ_r, λ_c and λ_i represent the failure rates of the ended rectifier, clamped capacitor and inverter, respectively. The failure rates of the rectifier and inverter can be calculated as [36]:

$$\lambda_r = 6 \times (\lambda_{thyristor} + \lambda_{diode}), \tag{31}$$

$$\lambda_i = 6 \times (\lambda_{IGBT} + \lambda_{diode}), \tag{32}$$

where $\lambda_{thyristor}$, λ_{diode} and λ_{IGBT} are failure rates of thyristors, diodes and IGBTs, respectively. To calculate these failure rates, Equation (22) is used. However, the associated parameters such as activation energy, base failure rates, thermal losses and current passes through them that are used in this equation to determine the failure rate of thyristors, diodes or IGBTs are different. The failure rate of the capacitor placed between the rectifier and the inverter can be determined as [11]:

$$\lambda_C = \lambda_0\pi_T\pi_C\pi_V\pi_{SR}\pi_E, \tag{33}$$

where λ_0, π_T, π_C, π_V, π_{SR} and π_E are the base failure rate of the capacitor at the test condition, temperature factor, capacitance factor, voltage stress factor, series resistance factor and environmental factor, respectively.

According to the IEC 60076–7, the temperature of an oil-type transformer widely used in the power system considering the winding current can be determined as [37]:

$$T_{tr} = T_a + \Delta T_0 \left(\frac{1 + r_t a}{1 + r_t} \right)^{\varkappa} + H g_r a^{y}, \tag{34}$$

where T_{tr} is the temperature of the transformer in winding current (I_{tr}), ΔT_0 is the rate of change of transformer temperature in steady state despite nominal losses, r_t indicates the ratio of load losses in rated current and no load losses, $\varkappa$ and y are the oil and coil power coefficients, H represents the hot spot factor, g_r is used to model the average-winding-to-average-oil at rated current and a is the ratio of the winding current over the rated current. Equation (21) shows the inductive voltage of a transformer in which the current of the inverter is considered to be the same as the current of the transformer. It is worth noting that wind speed changes are also included. According to the Arrhenius law, the failure rate of the transformer considering the variable temperature ascended from the difference in the ambient temperature and wind speed can be determined. The temperature rise of a cross-linked polyethylene (XLPE) cable widely utilized in the power system considering the cable current can be determined as [38]:

$$\Delta T = T_1 \left(rI^2 + \frac{W_d}{2} \right) + nT_2(W_d + rI^2(1 + \sigma_1)) + n(T_3 + T_4)(W_d + rI^2(1 + \sigma_1 + \sigma_2)), \tag{35}$$

where T_1, T_2, T_3 and T_4 are the thermal resistances between different layers of the cable. If the number of layers used in the understudied cable is less than the numbers considered in the model, two or more of the layers coincide, and so, the corresponding thermal resistance will be zero. Besides, σ_1 and σ_2 are relative losses between different layers of the cable; W_d is the dielectric losses, r is the resistance of the cable conductor at maximum operation temperature, I is the cable current and n is the number of conductors in the cable. According to the Arrhenius law, the failure rate of the XLPE cable, considering different temperature associated to the different ambient temperature and different currents ascended from the variation in the wind speed can be investigated.

3.2 | The failure rate of tidal turbine

To evaluate the tidal generation unit failure rate considering the components failure rate, the procedure similar to the wind turbine failure rate determination is followed. The failure of the main components of the tidal unit including tidal turbine, gearbox, DFIG, electrical converters, control system, transformer and cable results in the failure of the overall power plant and so, these components are in series in the reliability model of the unit. Thus, the equivalent failure and repair rates of the tidal generation unit can be determined as (2) and (3), respectively. In this stage, the dependency of tidal unit components on the tidal current speed is determined. The relationships that indicate the dependency of the wind turbine gearbox and turbine failure rates on rotational speed and temperature are also established for gearboxes and turbines used in the tidal turbines. However, to determine the failure rate of the gearbox and turbine used in the tidal units, the wind speed is replaced by tidal current speed and the ambient temperature is replaced by seawater temperature. Biofouling is one of the factors that has a great impact on the performance and failure of tidal turbines, especially horizontal axis types. In [39], the roughness effect on the performance of horizontal axis tidal turbines that is arisen from biofouling is studied. For this purpose, a computational fluid dynamic-based unsteady Reynolds Averaged Navier–Stokes simulation model is used to predict the impact of biofouling on a full-scale horizontal axis tidal turbine. It is concluded from [39] that increase in biofouling result in decrease in power coefficient (C_P) of tidal turbines. The power coefficient of tidal turbine is defined as the ratio of the actual power produced by the tidal turbine to its theoretical power. According to the biofouling condition of the understudied site that the tidal turbine is installed there, the power coefficient of the tidal turbine is determined and used to calculate the generated power and reliability parameters of the understudied tidal turbine.

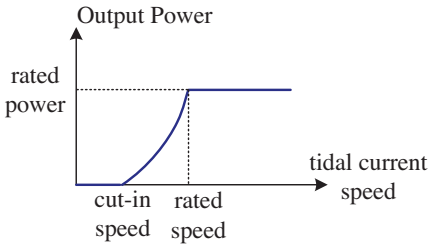

FIGURE 10 The power curve of tidal turbines

To evaluate the failure rate of the DFIG used in the tidal generation units, at first, the produced energy of the generator considering the tidal current speed is obtained using of the power curve of the tidal turbine, as can be seen in Figure 10. As can be observed in the figure, because the speed of tidal currents is low, the speed does not reach the cut-out speed. The speed of the tidal turbine and generator rotor considering the tidal current speed is shown in Figure 11.

The rotor and the stator powers can be calculated as [36]:

$$P_r = -\frac{s}{1 - s} P_{out}, \tag{36}$$

$$P_s = \frac{1}{1 - s} P_{out}, \tag{37}$$

where s, P_r, P_s and P_{out} are slip, rotor power, stator power and DFIG output power. The slip can be determined as [36]:

$$s = \frac{n_s - n_r}{n_s} = \frac{v_s - v_{tid}}{v_s}, \tag{38}$$

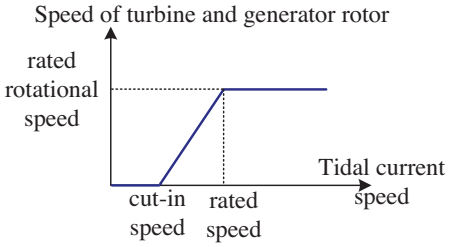

FIGURE 11 The speed of tidal turbine and generator rotor versus tidal current speed

where n_s, n_r, v_s and v_{tid} are the rotational synchronous speed in rpm, the rotational speed of the rotor, the tidal current speed associated to the synchronous speed in m/s and the tidal current speed, respectively. The induced voltage in the rotor can be determined as [36]:

$$V_r = sV_s\frac{N_r}{N_s}, \tag{39}$$

where V_r, V_s, N_s and N_r are rotor voltage, stator voltage, the number of stator winding turns per phase and the number of rotor winding turns per phase. To determine the failure rate of the DFIG, mechanical and electrical parts failure rates must be determined and combined as (15). The currents of rotor and stator windings can be determined by dividing the rotor and stator powers by the associated voltages. The power losses associated to the stator and rotor windings can be calculated as [15]:

$$P_{loss\text{-}stator} = 3r_sI_s^2, \tag{40}$$

$$P_{loss\text{-}rotor} = 3r_rI_r^2, \tag{41}$$

where $P_{loss\text{-}stator}$, $P_{loss\text{-}rotor}$, r_s, r_r, I_s and I_r are the power losses of the stator windings, the power losses of the rotor windings, stator resistance per phase, rotor resistance per phase, stator current and rotor current, respectively. The temperature of the stator and rotor can be determined using of the thermal modelling of the generator as [36]:

$$T_s = T_{seawater} + R_{GHS}P_{loss\text{-}stator}, \tag{42}$$

$$T_r = T_{seawater} + R_{GHR}P_{loss\text{-}rotor}, \tag{43}$$

where T_s, T_r, $T_{seawater}$, R_{GHS} and R_{GHR} are stator temperature, rotor temperature, the temperature of the seawater, equivalent thermal resistance of the stator windings to the body and equivalent thermal resistance of the rotor windings to the body. According to the Arrhenius law, the failure rate of the DFIG considering the temperature rise of the stator and rotor windings can be determined. The dependency of the failure rate of the DFIG arisen from the mechanical parts on the tidal currents speed can be determined in a manner similar to the wind turbine.

To evaluate the failure rate of the electrical converters used in the tidal turbines, a manner similar to the wind turbines is utilized and Equations (16)–(29) are used. However, in the tidal or wind turbines based on the DFIG technology, the current of the rectifier is the rotor current and the peak current of the inverter can be calculated as [36]:

$$I_{P\text{-}inverter} = \frac{\sqrt{2}P_r}{\sqrt{3}V_s}. \tag{44}$$

For determination, the failure rates of the transformer and the cable used in the tidal turbines, the same procedure discussed for the wind turbines is followed and Equations (31) and (32) can be used.

3.3 | The failure rate of the PV system

The structure of a typical PV system is presented in Figure 12. As can be seen in the figure, a PV panel is composed of several branches with series solar cells. A PV system composed of several PV arrays can be connected to the microgrid through an inverter, transformer and cable. In addition to the inverter, a DC to DC converter can be used in the PV system structure to track the maximum power point. However, in the modern PV systems, in addition to convert DC power to AC, the inverters can perform the function of MPPT converter and so, the associated DC to DC converter can be removed. In this study, it is assumed that the inverter used in the PV system can perform both functions including tracking the maximum power point and DC to AC conversion. However, if there is an MPPT converter in addition to the inverter, its failure rate can be easily determined. The DC to DC converters consist of one or more diodes, capacitors and IGBTs. This paper develops the equations associated to determine failure rates of these devices and their dependency on the current passing through them. In this structure, a PV array is composed of several parallel strings with series panels.

If the transformer or cable fails, the entire system is likely to fail and the transmission power to the microgrid will be interrupted. In addition, the failure of any array of the PV system also leads to the failure of the part of the production source that contains the defective array. Therefore, the production capacity of the PV system can be determined by Equation (42) [24].

$$P_{PV} = \frac{n-1}{n}P_{string} = \frac{n-1}{n}mP_{panel}, \tag{45}$$

where P_{PV}, n, P_{string}, m and P_{panel} are the generated power of the PV system, the number of strings installed in the PV system, the generated power of each string, the number of series panels installed in each string and the generated power of each panel, respectively. The failure of each inverter results the generated power of the associated array would be zero. If a PV system is composed of n_a arrays, the failure of each array results the generated power of the PV system reduces to [24]:

$$P_{PV} = \frac{n_a-1}{n_a}P_{array}, \tag{46}$$

where P_{PV}, n_a and P_{array} are the generated power of the PV system, the number of arrays installed in the PV system and

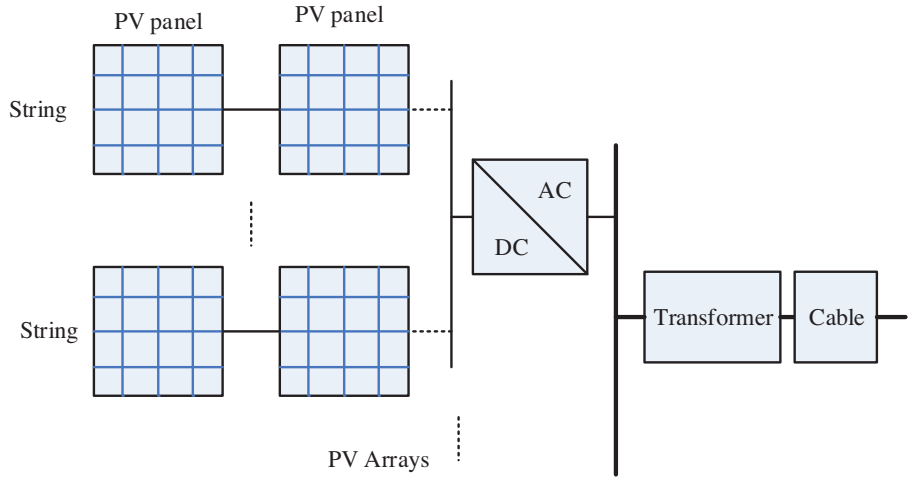

FIGURE 12 The structure of a typical PV system [38]

the generated power of each array, respectively. The generated power of the PV panels considering the variation in the solar radiation and the ambient temperature can be determined as [40]:

$$P_{panel} = \frac{s}{s_0} P_0[1 + \gamma_P(T_a - T_{a0})], \tag{47}$$

where s, s_0, P_0, γ_P, T_a and T_{a0} are the solar radiation, the solar radiation in the test condition, the generated power of the PV panel in the test condition, temperature coefficient of the power parameter, the ambient temperature and the ambient temperature in the test condition. In addition to the generated power, the voltage of the PV panel is dependent on the temperature as [40]:

$$V_{panel} = V_0[1 + \gamma_V(T_a - T_{a0})], \tag{48}$$

where V_0 and γ_v are the maximum power point voltage of the PV panel under standard test conditions and the temperature coefficient of the voltage parameter, respectively. The PV panels are composed of solar cells that are the p-n junctions. Thus, the failure rate of these components is determined in a manner similar to the other semiconductor devices as [11]:

$$\lambda_{sc} = \lambda_0 \pi_T \pi_S \pi_A \pi_R \pi_E, \tag{49}$$

where λ_{sc}, λ_0, π_T, π_S, π_A, π_R and π_E are the failure rate of the solar cell, the base failure rate of the solar cell, the temperature factor, the electric stress factor, the application factor, the power factor and the environmental factor. To determine the failure rate of the PV panel considering the variation in the temperature and generated power, the temperature factor, the electric stress factor and the power factor can be determined as [11]:

$$\pi_T = e^{\frac{-E_a}{k}\left(\frac{1}{T+273} - \frac{1}{298}\right)}, \tag{50}$$

$$\pi_s = \alpha e^{\beta V_{SC}}, \tag{51}$$

$$\pi_R = P_{sc}^a, \tag{52}$$

where α, β and a are constants associated to the specific solar cell, V_{sc} and P_{sc} are the voltage and the generated power of the solar cell. The application factor of the solar cell in the PV system is considered to be 1.5 and the environmental factor associated to the coastal area is considered to be 15 [11]. Dust is one of the important factors that have a great impact on solar panel failures. The higher the amount of dust on the PV panels, the higher the failure rate of the panels. For this purpose, according to the environmental conditions, the PV panels are periodically cleaned. In this study, the dust factor is included in the environmental conditions factor, and the greater the amount of dust, the greater this factor is considered. According to Equations (44)–(49), considering the variation in the solar radiation and ambient temperature the failure rate of the PV panel can be determined. The failure rates of the inverter, transformer and the cable can be calculated in a manner similar to the procedure discussed in wind and tidal turbines. Thus, according to the voltage and generated power of the PV array, the current and voltage of the inverter, transformer and cable are calculated and used to determine the failure rate of the PV system.

3.4 | The failure rate of central control system

In the central control system of the renewable energy-based microgrid, both hardware and software failures may be occurred. The hardware includes a few sensors, signal processors and different controllers, whereas the software refers to control programs. When either the software or hardware fails, the central control system fails. Thus, the failure rate of the central control system can be determined as [36]:

$$\lambda_{cc} = \lambda_h + \lambda_s, \tag{53}$$

where λ_{cc}, λ_h and λ_s are failure rates of control system, hardware and software, respectively. Due to the maturity of central control systems used in the renewable energy-based microgrids, it is often ignored from the software failure rates. Failure of

central control system results in the maloperation of the understudied microgrid and consequently failure of the microgrid. Thus, from reliability point of view, the renewable energy-based units and central control system are connected in series in the reliability model of the microgrid. Therefore, to calculate the equivalent failure rate of the microgrid, the failure rate of renewable energy-based units and failure rate of the central controller are added.

4 | IMPLEMENTATION OF THE PROPOSED METHOD IN PRACTICE

In the previous sections, the equations associated to the dependency of failure rate of composed components of the wind unit on the wind speed and air temperature, the failure rate of tidal unit components on the tidal current speed and water temperature, and the failure rate of the PV system on the solar radiation and air temperature are developed. To implement the proposed method and determine the failure rate of the renewable energy-based microgrid considering the wind speed, tidal current speed, solar radiation and temperature the following procedures are suggested:

- Input required data including hourly wind speed, tidal current speed, air and water temperature, solar radiation and associated parameters of all composed components of the renewable resources of microgrid.
- Determine the hourly failure rate of composed components of wind unit considering the hourly wind speed and air temperature based on the equations developed Section 3.1.
- Determine the hourly equivalent failure rate of wind unit using of Equation (2).
- Calculate the hourly failure rate of composed components of tidal unit considering the hourly tidal current speed and water temperature based on equations developed in Section 3.2.
- Calculate the hourly equivalent failure rate of tidal unit.
- Calculate the hourly failure rate of composed components of PV system considering the hourly solar radiation and air temperature based on equations developed in Section 3.3.
- Determine the equivalent hourly failure rate of PV system.
- Calculate the hourly equivalent failure rate of the microgrid considering equivalent failure rate of wind unit, tidal turbine, PV system and central controller using Equation (2).

The flowchart associated to determine the equivalent failure rate of the renewable energy-based microgrid during a year is presented in Figure 13. In the previous sections, a renewable energy-based microgrid containing of the wind turbines, current type tidal turbines and PV systems is considered and the resource-dependent failure rates of the main components are developed. To clearly study the impact of the variation in the wind speed and air temperature on the failure rate of the wind energy system components comprising the wind turbine, gearbox, PMSG, back-to-back converter, control system, transformer and cable, numerical results are performed. For the current type tidal turbine, the impact of the variation in the

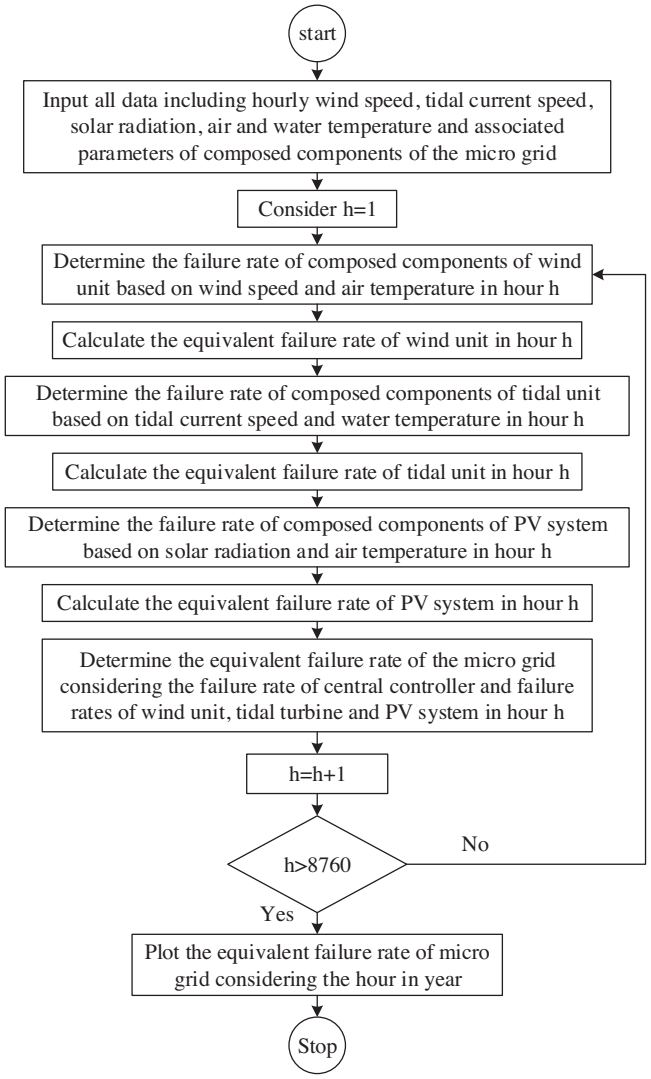

FIGURE 13 The flowchart associated to implement the proposed method in practice

tidal current speed and water temperature on the failure rate of the main components including the tidal turbine, gearbox, DFIG, electrical converters, control system, transformer and cable is obtained. For the PV system, the failure rate of the main energy conversion components including the PV panels, electrical converters, control system, transformer and cable taken into account the variation in the solar radiation and air temperature is developed. Then, a reliability performance assessment approach according to the Monte Carlo simulation method is presented in this part, to evaluate the reliability of the renewable energy-based microgrids considering the variable failure rate of the main components ascended from the variation in the renewable resources and environment temperature. In the current paper, moreover, the influence of some types of renewable energy sources on the failure rate of the whole system is taken into account by considering the effect of temperature.

To study the reliability performance of this renewable energy-based microgrid considering only the effect of the generation units, the distribution and transmissions network are considered

to be 100% reliable and thus, it is neglected from the failure of the transmission lines, the equipment of the substations and distributions lines. The structure of the understudied renewable energy-based microgrid composed of the wind turbines, current type tidal units and PV panels for reliability performance studies is presented in Figure 1. As can be seen from the figure, for reliability evaluation of the renewable energy-based microgrid, all generation units and moreover, all different types of loads are connected to a single common bus and it is neglected from the failure of other parts.

To evaluate the reliability of the renewable energy-based microgrid including wind and tidal turbines, PV system and load, the following procedure according to the Monte Carlo simulation approach is presented here:

Step1. The input data including hourly wind speed, hourly tidal current speed, hourly solar radiation, hourly temperature, hourly load during one or more years, the characteristics of the wind turbines, tidal turbines, PV systems and central controller and the reliability data associated to the components must be collected.

Step2. According to the equations associated to the components failure rate developed in, in a given hour based on the collected data, the failure rate is computed for all system components.

Step3. The hourly probabilities of up or down states for the main components will be calculated according to the hourly failure and repair rates of them.

Step4. In each hour, for all components, a random number located in the interval [0,1] is produced. If the produced number is in the intervals [0,P_{up}] or [P_{down},1], the component is considered to be up. However, if the generated number is in [P_{up},1] or [0,P_{down}], the components would be down.

Step5. According to the reliability models of generation units obtained in Section 3, the impact of each component on the failure of the generation units is determined. Thus, the states of the generation units and associated generated powers in the understudied hour are determined. The central controller is the key component of the model. Failure of this component results in the overall failure of the microgrid and consequently zero production power. Thus, if the generated number associated to this component results in its failure, the generated power of the microgrid would be zero.

Step6. By comparing the hourly production capacity of the microgrid with the hourly load, the amount of hourly interrupted load is determined.

Step7. By repeating the simulation method over several thousand years, the average value of reliability indices is calculated as follows [25]:

$$LOLP = \frac{\sum_{k=1}^{n\times 8760} B_k}{n \times 8760}, \tag{54}$$

$$LOLE = \frac{\sum_{k=1}^{n\times 8760} B_k}{n}, \tag{55}$$

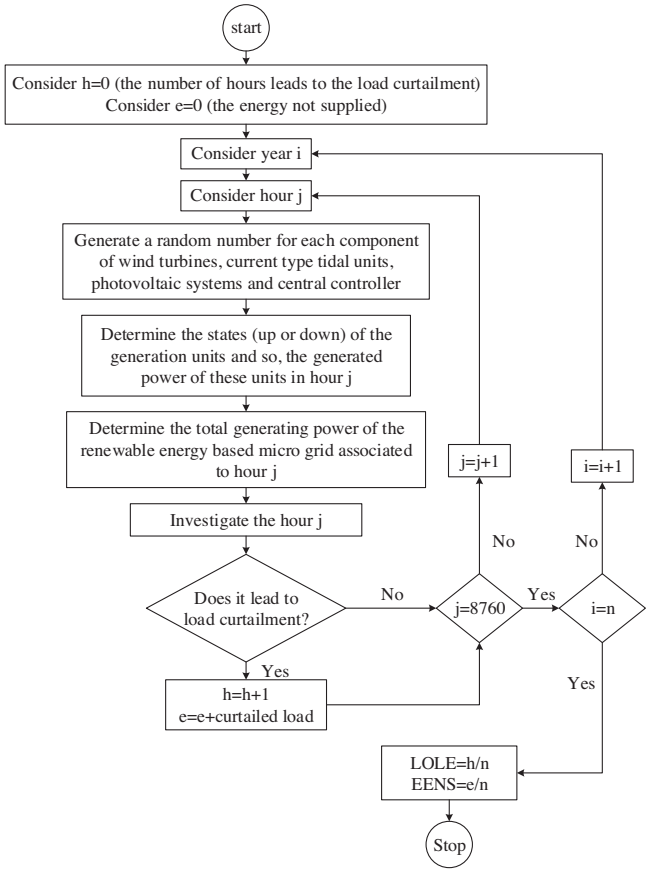

FIGURE 14 The flowchart of reliability evaluation method

$$EENS = \frac{\sum_{k=1}^{n\times 8760} L_k}{n}, \tag{56}$$

where *LOLP, LOLE, EENS,* B_k, n and L_k are loss of load probability, loss of load expectation in hours per year, expected energy not supplied in MWh per year, a binary number, number of simulated years and the hourly interrupted load in MW. The binary number B_k can be determined as [25]:

$$B_k = \begin{cases} 1 & P_{microgrid,k} < load_k, \\ 0 & P_{microgrid,k} \geq load_k, \end{cases} \tag{57}$$

where $P_{microgrid,k}$ and $load_k$ are the microgrid generated power loads at hour k, respectively. The flowchart of the proposed method to evaluate the reliability of the renewable energy-based microgrid is presented in Figure 14.

5 | SIMULATION RESULTS

5.1 | The impact of resource variation on the components failure rate

In this part, the impact of the variation in the renewable resources including the wind speed, the tidal current speed and solar radiation and also the variation in the environment

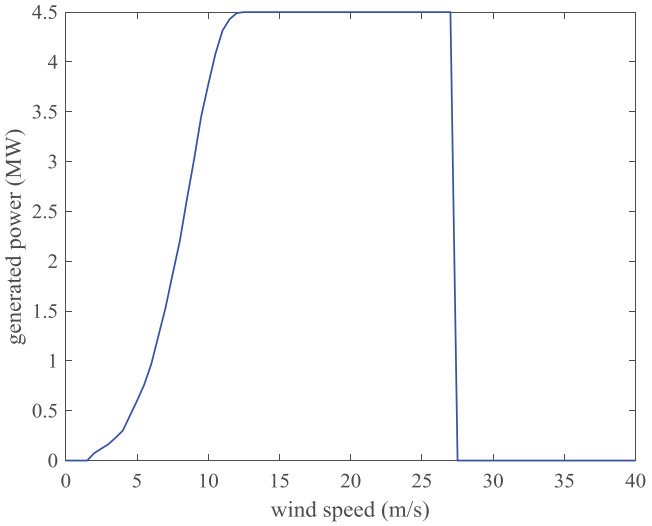

FIGURE 15 The power curve of the understudied wind turbines [41]

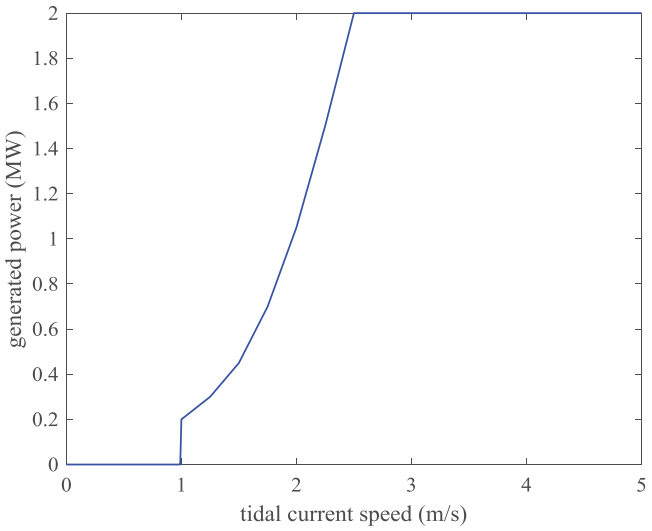

FIGURE 16 The power curve of the understudied current type tidal turbines [42]

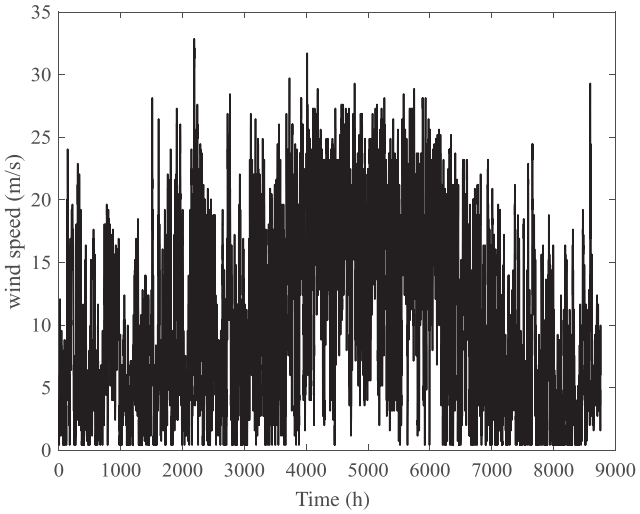

FIGURE 17 The hourly wind speed [43]

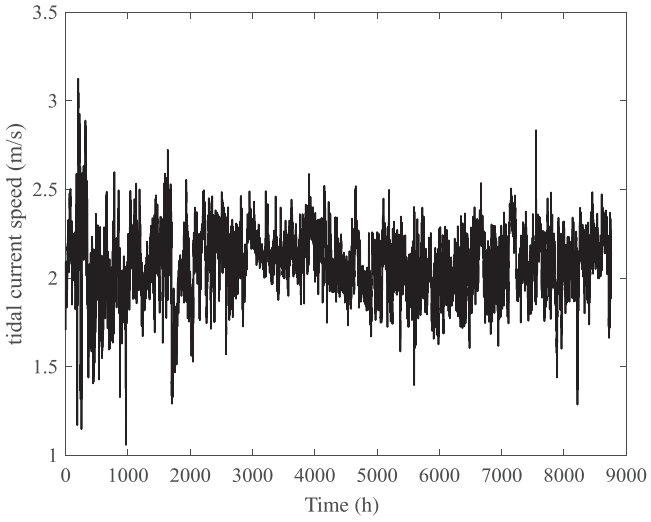

FIGURE 18 The hourly tidal current speed [43]

temperature including the air and water temperature on the main components failure rate for the wind energy system, current type tidal units and PV systems is studied. In this paper, to focus on the impacts of variation in the renewable resources and temperature on the failure rate of composed components of renewable energy-based units, the central control system is assumed to be 100% reliable.

In the reliability evaluation of this paper, a microgrid including a wind turbine with 4.5 MW capacity, a tidal turbine with 2 MW capacity and a PV system composed of 4000 panels with 1 MW capacity is considered to be installed in a coastal area. The power curve of the wind and tidal turbines are presented in Figures 15 and 16, respectively [41–42]. In the PV system, there are 10 arrays that each array includes 25 parallel strings. Each string contains 16 series panel, that each panel includes 36 series solar cells. The generated power of each PV panel in solar radiation of 900 w/m^2 and air temperature of 25°C would be 250 W. The hourly wind speed, tidal current speed, solar radiation, air temperature, water temperature and load during the year 2018 are presented in Figures 17–22, respectively [43–44]. As can be seen in the figures, the renewable resources including the wind speed, tidal currents speed, solar radiation and also the environment temperature change a lot in time and it is expected that the system components failure rate of the microgrid including different types of renewable energy resources is influenced suggestively. Therefore, it is expected that the reliability performance in the considered power grid will be calculated and evaluated more accurately. The variation in the load is considered to be based on the IEEE load patterns [44].

According to the hourly wind speed, tidal current speed, solar radiation data and air temperature data, and based on the power curve of the wind and tidal turbines and the number of PV

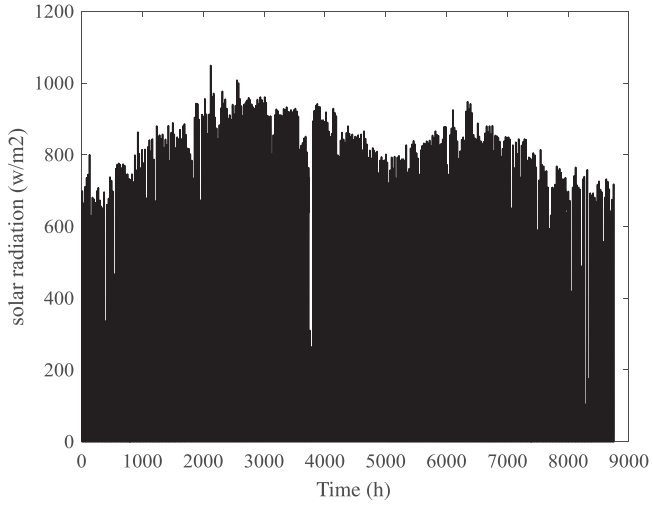

FIGURE 19 The hourly solar radiation [43]

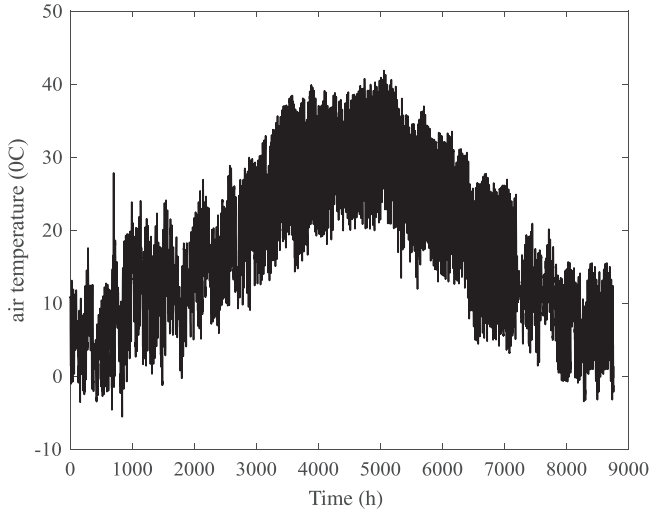

FIGURE 20 The hourly air temperature [43]

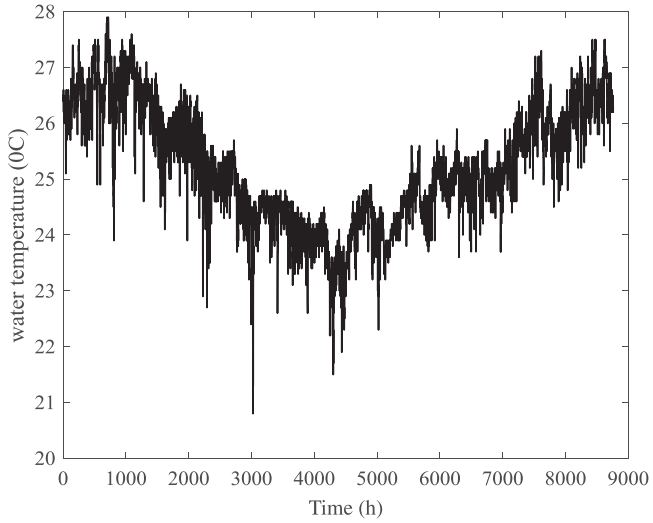

FIGURE 21 The hourly water temperature [43]

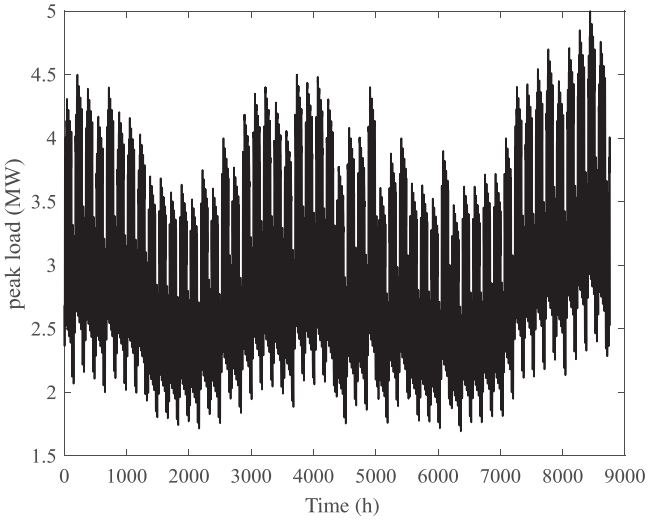

FIGURE 22 The hourly peak load [44]

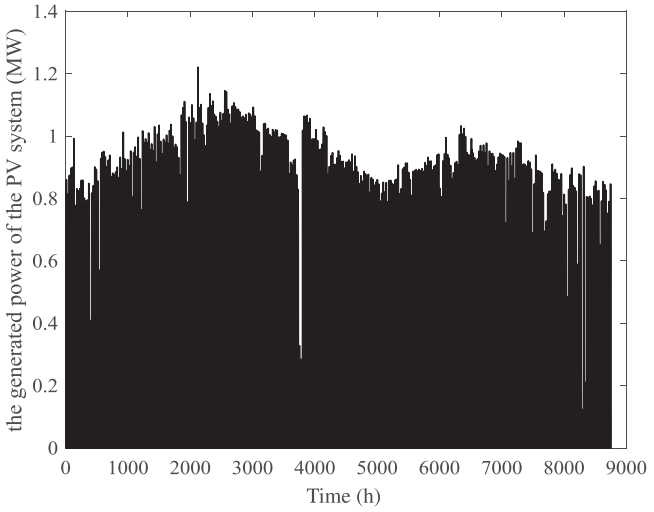

FIGURE 23 The hourly PV power

panels, the generated power of power generation sources including PV system, wind and tidal turbines and also the voltage of the PV system is determined and presented in Figures 23–26, respectively. As observed in Figure 23, due to the fluctuation in the solar radiation and ambient temperature, the generated power of the PV system changes, correspondingly. Also, it is deduced from Figures 24 and 25, due to the fact that wind speed and tidal currents speed are not constant, their output power will also change, accordingly.

According to the model presented in this paper, the output voltage of the PV panels depends on the ambient temperature, non-linearly. According to Figure 26, it is observed that the output voltage of PV panels changes with temperature variation. In this part of the paper, the failure rate for the main components of the wind turbine and tidal energy systems is determined according to changes in wind speed, ambient temperature, and water temperature. It is noteworthy that the variation in the reliability indices of the PV system are likewise dependent on wind

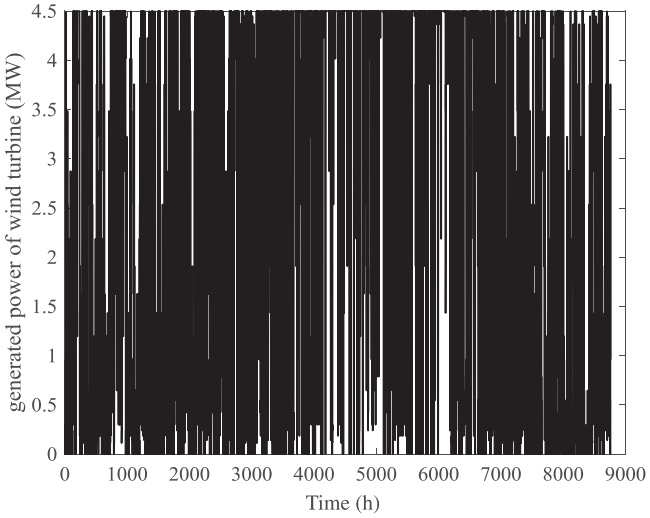

FIGURE 24 The hourly power of wind turbine

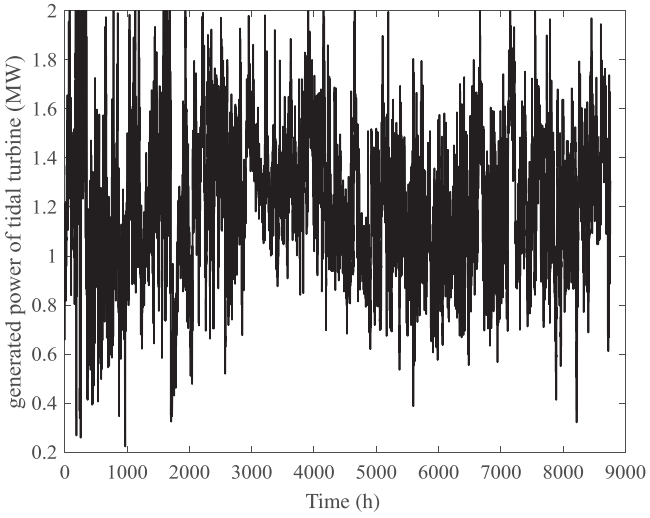

FIGURE 25 The hourly power of the current type tidal turbine

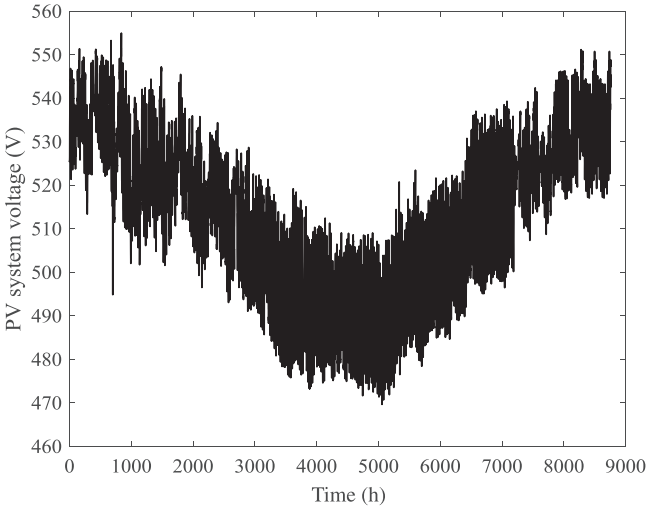

FIGURE 26 The hourly PV voltage

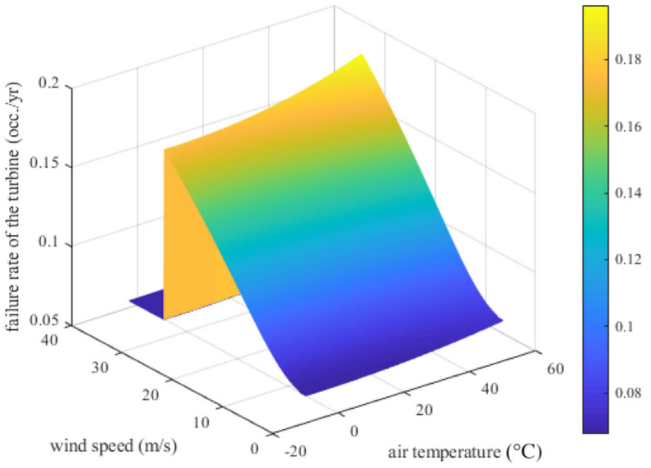

FIGURE 27 The variation of the wind turbine failure rate considering the variation in the wind speed and air temperature

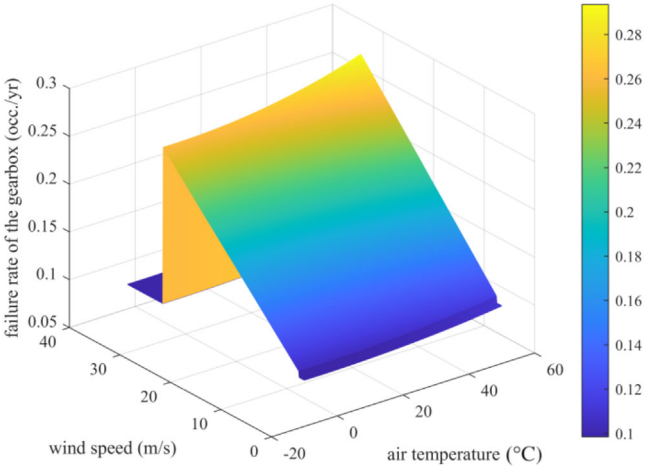

FIGURE 28 The variation of the gearbox failure rate considering the variation in the wind speed and air temperature

energy and tidal systems, and according to developed equations presented in this paper, the changes in solar radiation and ambient temperature, which affect the output power of PV arrays, will also have a corresponding effect. Since the failure rate of main components of the wind generation units including the wind turbine, the gearbox, the PMSG, the electrical converters, the transformer and the cable changes according to the variation in the wind speed and air temperature, the outputs are presented in Figures 27–32, respectively. The compulsory parameters to study the failure rates of composed components are obtained from the model presented in [26–44]. These required data are presented in Table 1 [26–44]. As can be understood from the figures, the failure rate of the mechanical parts of the wind energy system including the wind turbine, gearbox and rotor is considerably dependent on the rotation speed. Consequently, the growth in the rotation speed of these components results in the increase in the calculated failure rate. In addition, the figures show that lowering the temperature does not have much

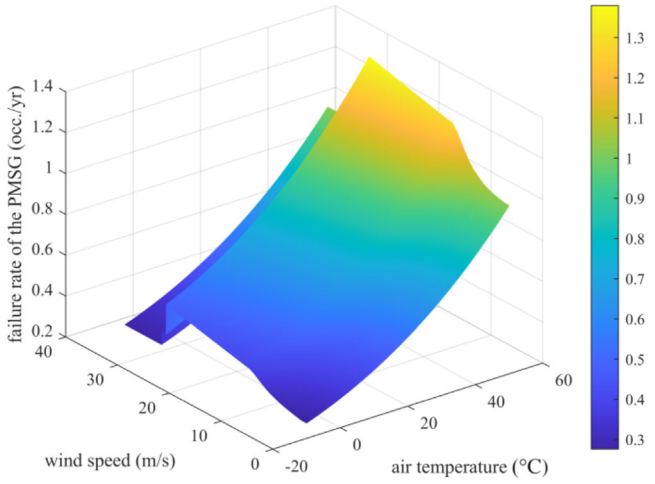

FIGURE 29 The variation of the PMSG failure rate considering the variation in the wind speed and air temperature

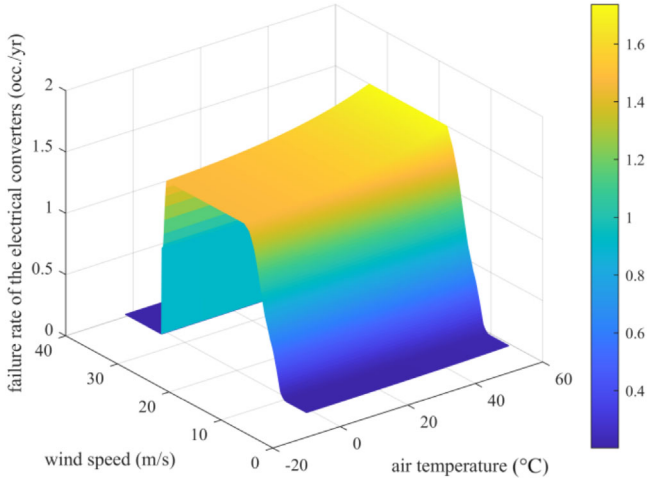

FIGURE 30 The variation of the back-to-back converter failure rate considering the variation in the wind speed and air temperature

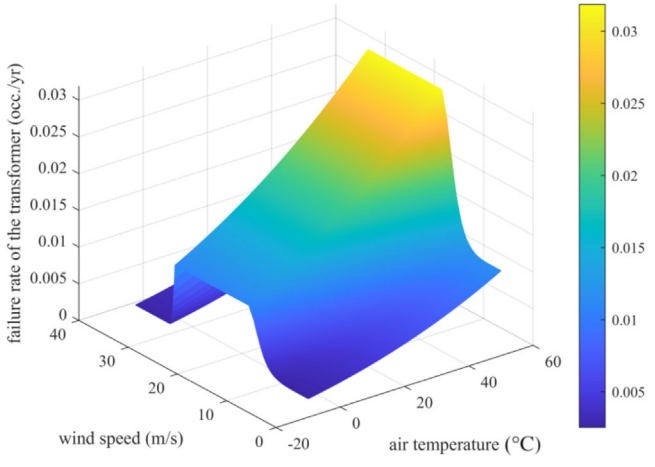

FIGURE 31 The variation of the transformer failure rate considering the variation in the wind speed and air temperature

TABLE 1 The component data [26–44]

Parameter	Value
Modulus of the spar section	0.00073 m^3
Spar material strength	350 MPa
Generator activation energy	0.2
Boltzmann constant	0.00008617 ev/K
Stator winding resistance of PMSG	0.04 ohm
Thermal resistance of generator	2 K/kW
Thermal resistance of interface to heat sink	0.55 K/kW
Thermal resistance of interface to junction	23 K/kW
Switching frequency	3 kHz
Voltage drop on diodes	0.7 V
Voltage drop on thyristors	1.3 V
Voltage drop on IGBTs	1.5 V
Reference voltage	0.9 V
DC link voltage	1.2 kV
Resistance of diodes and thyristors	0.09 ohm
Resistance of IGBTs	0.06 ohm
Modulation index	0.5
Base failure rate of conducting condition	0.0001306
Base failure rate of non-conducting condition	0.001589
Base failure rate of temperature effect	0.00053
Solder joint failure rate	0.00295
Operating activation energy	0.3
Non-operating activation energy	0.4
DC_{op}	0.23
DC_{nonop}	0.77
DT	80
Base failure rate of capacitor	0.00021
Oil power coefficient of transformer	0.8
Coil power coefficient of transformer	1.3
Hot spot factor	1.1
g_r	14.5 K
r_t	6
Activation energy of transformer	0.2
T_1 for cable	0.90798 km/W
T_2	0
T_3	0.098588 km/W
T_4	0.0817 km/W
Dielectric loss	12.73
Cable activation energy	0.2
Rotor resistance of DFIG	0.1 ohm
Stator resistance of DFIG	0.03 ohm
Thermal resistance of stator	6 K/kW
Thermal resistance of rotor	15 K/kW
Temperature coefficient of the power parameter of PV panel	0.35
Temperature coefficient of the voltage parameter of PV panel	0.25

(Continues)

TABLE 1 (Continued)

Parameter	Value
Application factor	1.5
Environmental factor	15
Rated solar radiation	900 W/m^2
Rated power of solar panels	250 W
Number of PV panels	4000

effect on component failure, but if the temperature increases, the component failure rate will also increase sharply.

As can be seen from the figures, the rate of failure for the electrical components of the wind generation units including the PMSG, back-to-back converter, transformer and cable is dependent on the temperature rise of the components. The temperature increment of these components can be resulted from the growth in the ambient temperature and the thermal loss caused by the increasing in the electrical current flowing through them. Thus, the increase in the air temperature results in the increase in the failure rate of the PMSG, electrical converter, transformer and cable as can be seen from the figures. On the other hand, the current passing through the components resulted in the heat loss in the associated components is proportional to the produced energy by the wind turbine. Thus, as understood from the Figures 29–32, the shape of the failure rate curve associated to the electrical components of the wind turbine is very similar to the power curve of the wind turbine, which indicates the amount of the power output at different wind speeds.

Based on the equations developed in this paper, the failure rate of components used in the current type tidal generation system including the tidal turbine, gearbox, DFIG, electrical converters, transformer and cable considering the variation in the tidal current speed and the environment temperature are mathematically computed and represented in Figures 33–38, respectively. As can be seen in the figures, the failure rate of the

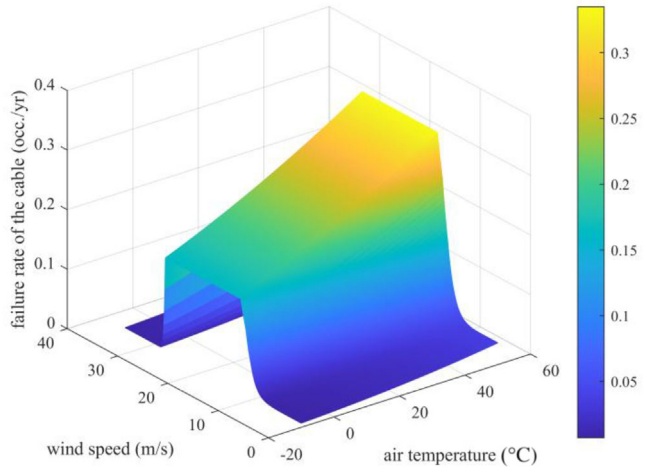

FIGURE 32 The variation of the cable failure rate considering the variation in the wind speed and air temperature

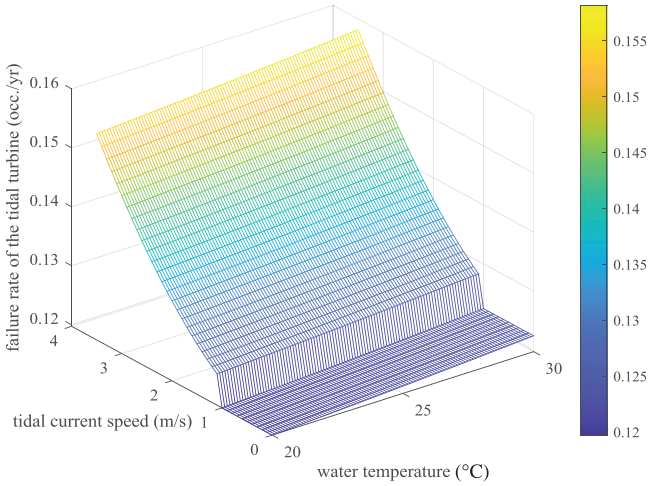

FIGURE 33 The variation of the tidal turbine failure rate considering the variation in the tidal current speed and water temperature

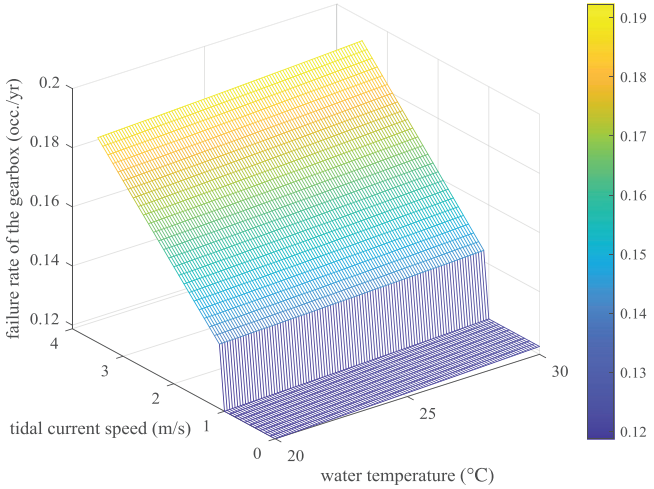

FIGURE 34 The variation of the gearbox failure rate considering the variation in the tidal current speed and water temperature

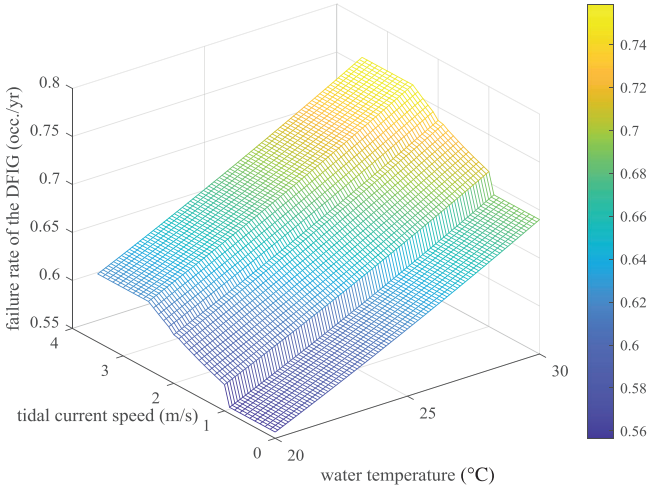

FIGURE 35 The variation of the DFIG failure rate considering the variation in the tidal current speed and water temperature

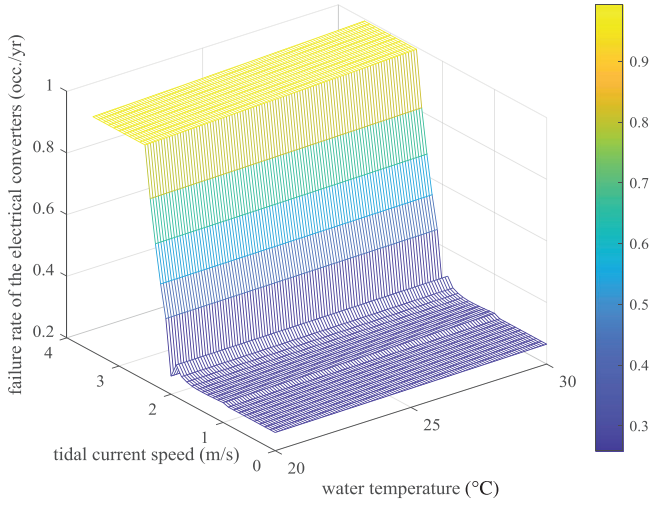

FIGURE 36 The variation of the back-to-back converter failure rate considering the variation in the tidal current speed and water temperature

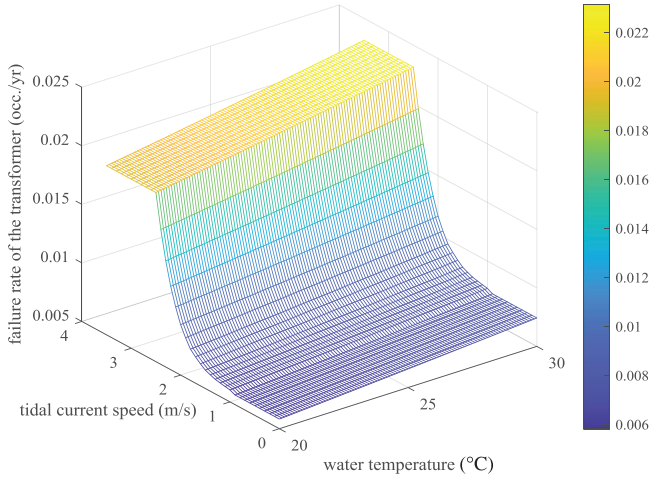

FIGURE 37 The variation of the transformer failure rate considering the variation in the tidal current speed and water temperature

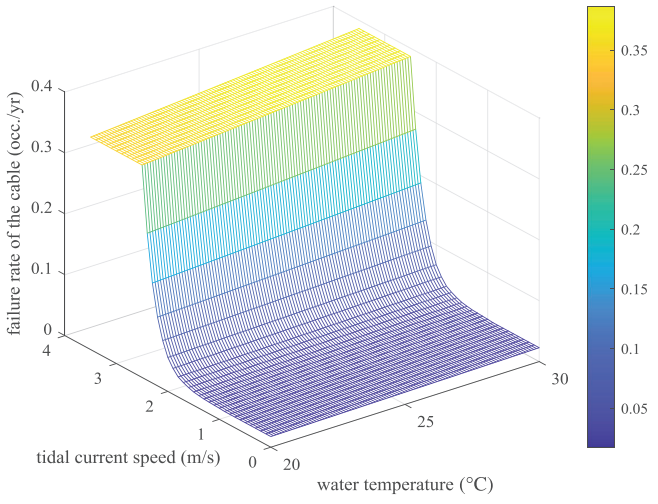

FIGURE 38 The variation of the cable failure rate considering the variation in the tidal current speed and water temperature

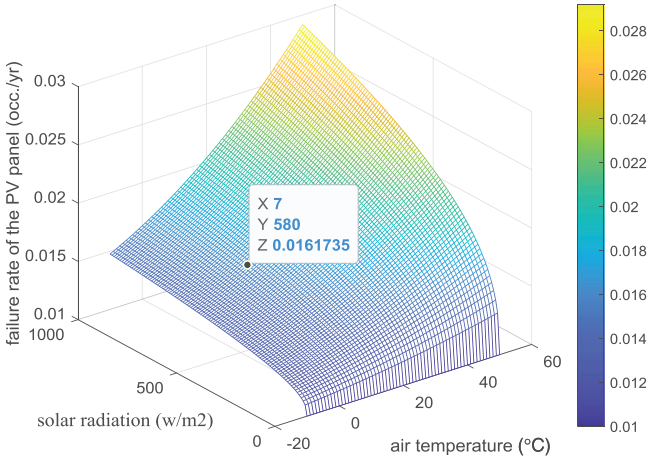

FIGURE 39 The variation of the PV panel failure rate considering the variation in the solar radiation and air temperature

mechanical components of the unit including the tidal turbine, the gearbox and the DFIG rotor significantly depends on the rotation speed and to a lesser extent depends on the temperature. Thus, the failure rate of the mechanical components of the tidal turbine significantly increases with increasing the rotation speed. On the other hand, with increasing water temperature, the failure rate increases slightly.

Similar to the wind turbine components, the failure rate of the electrical system components of the current type tidal unit comprising the DFIG, back-to-back converter, transformer and cable is dependent on the temperature rise of them. The temperature rise of the electrical components of the tidal generation unit is arisen from two reasons including the temperature rise of the water and the temperature rise caused by heat loss. The heat loss of the components is caused by current passing through them that is proportional to the generated power of the tidal power plant. Thus, the shape of the failure rate curve of electrical components including DFIG, electrical converters, transformer and cable would be resemble to the power curve diagram of the tidal turbine which shows the association between the produced power and the tidal current speed. This can be clearly seen in Figures 36–38.

The reliability performance evaluation for main system components of the PV structure under consideration including the PV panels, inverter, transformer and cable are achieved. The failure rate results of these devices regarding the variation of the solar radiation and air temperature are calculated and presented in Figures 39–42.

It is realized from the diagrams shown in the figures that the failure rate for the components of the PV system increases with growth in the solar radiation and air temperature. It is due to the temperature rise of the composed components of the PV system including the PV panels, inverter, transformer and cable. The temperature rise of these components is caused by two reasons including the temperature rise of the environment and the temperature rise arisen from the heat loss of the associated components due to the current passing through them. With increasing the solar radiation, the generated power of the

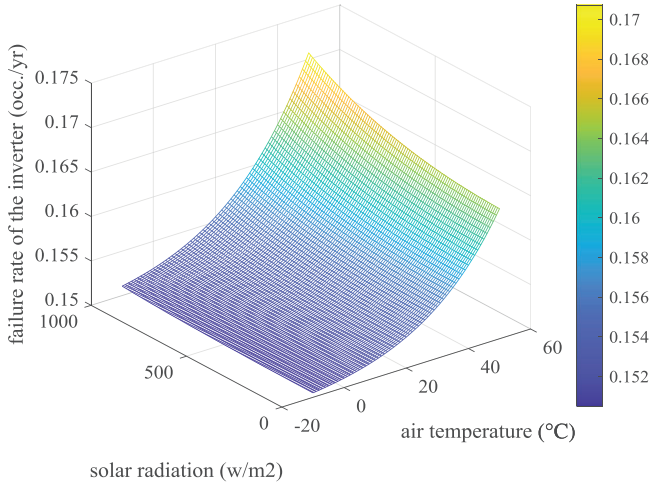

FIGURE 40 The variation of the inverter failure rate considering the variation in the solar radiation and air temperature

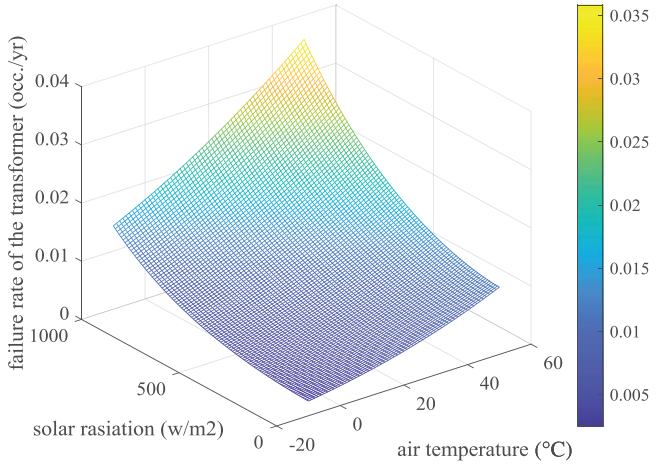

FIGURE 41 The variation of the transformer failure rate considering the variation in the solar radiation and air temperature

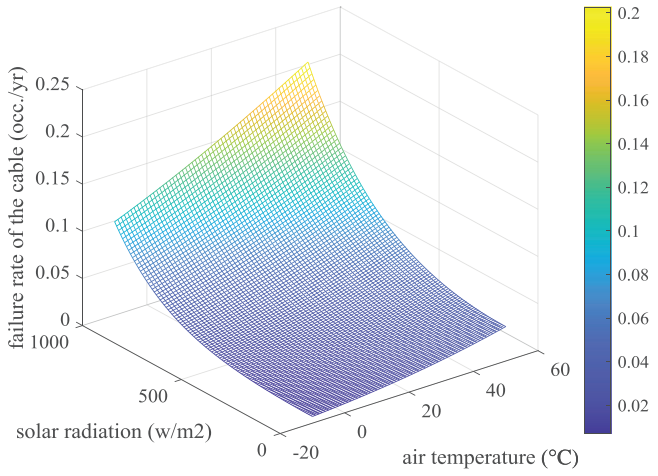

FIGURE 42 The variation of the cable failure rate considering the variation in the solar radiation and air temperature

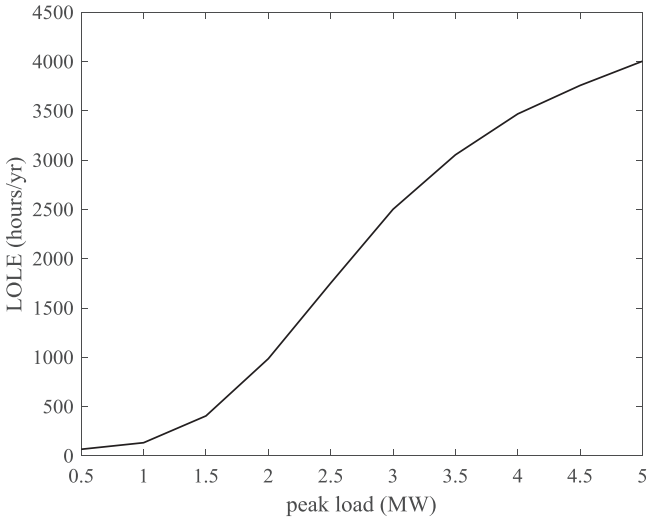

FIGURE 43 The loss of load expectation considering the peak load variation

PV system and consequently the current passing through the composed components increases, and so, the failure rate of the composed components of the PV system increases, too.

5.2 | Reliability assessment of the microgrid including renewable energy resources

In this subsection, in order to evaluate the proposed method and its applicability, reliability evaluation of a microgrid including a wind turbine with 4.5 MW capacity, a tidal turbine with 2 MW capacity and a PV system composed of 4000 panels with 1 MW capacity is performed. For reliability analysis of the understudied microgrid, the proposed variable failure rate of the components is applied. For this purpose, the Monte Carlo simulation approach with 1000 repetitions is used. The hourly failure rate of the components of the generation units is determined considering the variable hourly wind speed, tidal current speed, solar radiation, and air and water temperature during the understudied year as shown in Figures 17–21. Using of the hourly failure rate of the components, produced power of the PV system, wind and tidal turbines, and the hourly peak load, the adequacy indices of the microgrid under consideration are calculated based on the proposed technique. These indicators include the LOLE and EENS which are drawn in Figures 43 and 44, respectively. As observed in the figures mentioned, although the power generation capacity of the understudied microgrid can be up to 7.5 MW and the maximum peak load of the microgrid is 4.5 MW, due to the variation of the renewable energy resources, the reliability decreases significantly with increasing the peak load. Due to variation in the renewable resources including the wind speed, the tidal current speed and the solar radiation, the generated power of the renewable energy-based generation units is less than the rated capacity in the more of times. Thus, to improve the reliability of the renewable energy-based microgrid, an energy storage system is required.

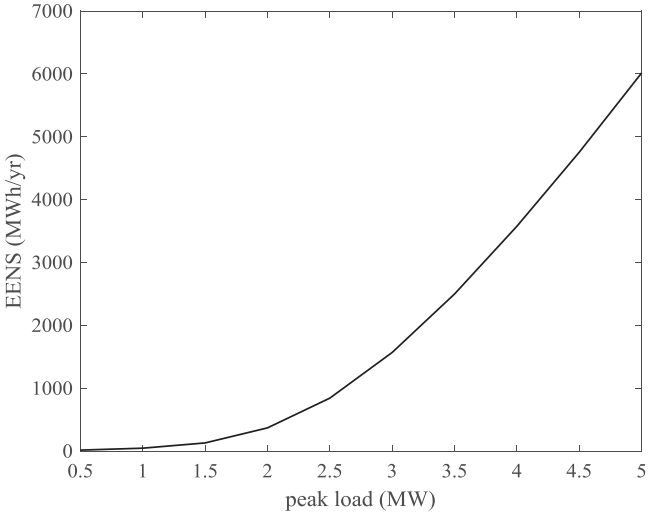

FIGURE 44 The expected energy not supplied considering the peak load variation

6 | CONCLUSION

In this paper, the dependency of the failure rates of the renewable energy-based microgrid on the variation in the renewable resources and temperature is determined that can be used for reliability evaluation of a renewable energy-based microgrid containing wind turbines, current type tidal generation units and PV systems. To consider the impact of the variable renewable resources on the failure rate of the microgrids, a comprehensive study is performed and the effects of the variation in the wind speed, tidal current speed, solar radiation, air and water temperature on the main components of these generation units including gearbox, turbine, generator, electrical converters, transformer, cable and PV panels are investigated. To determine the failure rate of the renewable energy-based microgrid, both effective electrical and mechanical components of the renewable energy-based generation units are considered and a comprehensive study is performed to determine an accurate resource-based failure rate. The resource-based equations of the components failure rates developed in this paper can be used for reliability assessment of a renewable energy-based microgrid to accurately study the impact of the variation in the wind speed, tidal currents speed, solar radiation and temperature on the reliability indices of the microgrids including wind turbines, current type tidal units and PV panels.

In the proposed framework, the reliability performance evaluation for a renewable energy based microgrid containing wind turbines, current type tidal generation units and PV systems is performed. As can be understood from the figures presented in this paper, the failure rate of the main components of the wind units, tidal turbines and PV systems are dependent on the renewable resources. Due to the significant variation of the renewable resources including wind speed, tidal current speed, solar radiation, air and water temperature, the failure rate of the associated components must be accurately determined to exactly evaluate the reliability of the microgrid containing these renewable generation units. Numerous results that can be used in the planning and operation of the renewable energy-based microgrids are deduced from the numerical analysis of the failure rates of the composed components. The failure rate of all components increases with increase in the air or water temperature. The failure of the mechanical components arisen from the reduction in the fatigue strength at higher temperature is determined by mechanical equations. The failure of the electrical components is increased due to the increase in the temperature according to the Arrhenius law. However, due to the different mixture of the electrical and mechanical parts of the studied components, the trends of the variation in the components failure rate is different. Due to the different structure of the PMSG and DFIG, different power curve of wind and tidal turbines and also different wind and tidal current speeds, the associated failure rate trends are different. It is clearly concluded from the figures that the trends of the failure rate for the modules of the wind energy system and tidal turbines are dependent on the shape of the power curve of these turbines. It is arisen from the dependency of the failure rate of the electrical components on the associated temperature rise and consequently the power losses of the components that are proportional to the corresponding current square. Furthermore, according to the numerical results obtained, it can be concluded that the temperature variation affects strongly the failure rate of the PV panels for the higher solar radiation. To examine the impact of the variable failure rates of the renewable energy-based generation units on the reliability performance of the microgrids, the numerical results calculated using of the Monte Carlo simulation approach are given. The numerical results represent that the failure rate of these generation units are significantly dependent on the renewable resources and so to exactly evaluate the reliability of the microgrids integrated to these resources, the proposed approach must be utilized.

In addition to the wind, tidal and solar energies, wave energy as one of the renewable resources that exists in different regions of the world, can be added to the renewable energy-based microgrids. In the future works, the dependency of failure rate of composed components of the wave converters on the wave height and wave period would be studied.

AUTHOR CONTRIBUTIONS

Ayoub Nargeszar: Conceptualization, Data curation, Formal analysis, Software, Supervision

Amir Ghaedi: Investigation, Methodology, Validation, Visualization, Writing – original draft

Mehdi Nafar: Investigation, Resources, Software, Writing – original draft, Writing – review and editing

Mohsen Simab: Investigation, Methodology, Validation, Writing – review and editing.

CONFLICT OF INTEREST

The authors declare that there is no conflict of interest that could be perceived as prejudicing the impartiality of the research reported.

FUNDING INFORMATION
The authors received no specific funding for this work.

DATA AVAILABILITY STATEMENT
Data available on request from the authors.

ORCID
Amir Ghaedi https://orcid.org/0000-0001-9959-7916

REFERENCES
1. Peyghami, S., et al.: Mission-profile-based system-level reliability analysis in DC microgrids. IEEE Trans. Ind. Appl. 55(5), 5055–5067 (2019)
2. Song, X., et al.: Reliability varying characteristics of PV-ESS-based standalone microgrid. IEEE Access 7, 120872–120883 (2019)
3. Guo, J., et al.: Reliability modeling and assessment of isolated microgrid considering influences of frequency control. IEEE Access 7, 50362–50371 (2019)
4. Guo, Y., et al.: Short-term reliability assessment for islanded microgrid based on time-varying probability ordered tree screening algorithm. IEEE Access 7, 37324–37333 (2019)
5. Song, X., et al.: A novel sequential sampling algorithm for reliability assessment of microgrids. IEEE Access 8, 134468–134479 (2020)
6. Said, S.M., et al.: SMES-based fuzzy logic approach for enhancing the reliability of microgrids equipped with PV generators. IEEE Access 7, 92059–92069 (2019)
7. Wang, S., et al.: New metrics for assessing the reliability and economics of microgrids in distribution system. IEEE Trans. Power Syst. 28(3), 2852–2861 (2013)
8. Patowary, M., Gayadhar, P., Deka, B.C.: Reliability modeling of microgrid system using hybrid methods in hot standby mode. IEEE Syst. J. 13(3), 3111–3119 (2019)
9. Xie, H., et al.: Optimal energy storage sizing for networked microgrids considering reliability and resilience. IEEE Access 7, 86336–86348 (2019)
10. Gautam, P., Piya, P., Karki, R.: Development and integration of momentary event models in active distribution system reliability assessment. IEEE Trans. Power Syst. 35(4), 3236–3246 (2020)
11. Tu, P., et al.: Hierarchical reliability modeling of an islanded hybrid AC/DC microgrid. In: IEEE International Conference on Probabilistic Methods Applied to Power Systems (PMAPS) (2018)
12. Li, P., Li, M.: A novel reliability assessment method of microgrid based on time correlation model. In: IEEE 3rd Conference on Energy Internet and Energy System Integration (EI2) (2019)
13. Abdulgalil, M.A., Khalid, M., Alshehri, J.,: Microgrid reliability evaluation using distributed energy storage systems. In: IEEE Innovative Smart Grid Technologies-Asia (ISGT Asia) (2019)
14. Bani-Ahmed, A., et al.: Reliability analysis of a decentralized microgrid control architecture. IEEE Trans. Smart Grid 10(4), 3910–3918 (2018)
15. Wu, X., et al.: An MILP-based planning model of a photovoltaic/diesel/battery stand-alone microgrid considering the reliability. IEEE Trans. Smart Grid 12(5), 3809–3818 (2021)
16. Peyghami, S., Fotuhi-Firuzabad, M., Blaabjerg, F.: Reliability evaluation in microgrids with non-exponential failure rates of power units. IEEE Syst. J. 14(2), 2861–2872 (2019)
17. Zhong, W., et al.: Reliability evaluation and improvement of islanded microgrid considering operation failures of power electronic equipment. J. Mod. Power Syst. Clean Energy 8(1), 111–123 (2019)
18. Muhtadi, A., et al.: Distributed energy resources based microgrid: Review of architecture, control, and reliability. IEEE Trans. Ind. Appl. 57(3), 2223–2235 (2021)
19. Ghaedi, A., et al.: Reliability evaluation of a composite power system containing wind and solar generation. In: IEEE 7th International Power Engineering and Optimization Conference (PEOCO) (2013)
20. Ghaedi, A., et al.: Toward a comprehensive model of large-scale DFIG-based wind farms in adequacy assessment of power systems. IEEE Trans. Sustainable Energy 5(1), 55–63 (2013)
21. Mirzadeh, M., Simab, M., Ghaedi, A.: Reliability evaluation of power systems containing tidal power plant. J. Energy Manage. Technol. 4(2), 28–38 (2020)
22. Uihlein, A., Magagna, D.: Wave and tidal current energy–A review of the current state of research beyond technology. Renewable Sustainable Energy Rev. 58, 1070–1081 (2016)
23. Enevoldsen, P., Xydis, G.: Examining the trends of 35 years growth of key wind turbine components. Energy Sustain. Dev. 50, 18–26 (2019)
24. Ghaedi, A., et al.: Incorporating large photovoltaic farms in power generation system adequacy assessment. Sci. Iran. 21(3), 924–934 (2014)
25. Billinton, R., Allan, R.N.: Reliability Evaluation of Power Systems, 2nd edn. Plenum, New York, NY, USA and London, UK (1994)
26. Hein, M., et al.: Reliability of gears–Determination of statistically validated material strength numbers. In: American Gear Manufacturers Association Fall Technical Meeting (2018)
27. Bhardwaj, U., Teixeira, A.P., Soares, C.G.: Reliability prediction of an offshore wind turbine gearbox. Renewable Energy 141, 693–706 (2019)
28. Rey, G., González, R.J., Frechilla Fernández, P.: Estimating Gear Fatigue Life. Gear Solutions (2007)
29. Beermann, S.: Reliability, Lifetime and Safety Factors. Gear Technology (2018)
30. Budynas, R.G., Nisbett, J.K.: Shigley's Mechanical Engineering Design, 8th edn. New York: McGraw-Hill (2008)
31. Val, D.V., Chernin, L., Yurchenko, D.Y.: Reliability analysis of rotor blades of tidal stream turbines . Reliab. Eng. Syst. Saf. 121, 312–326 (2014)
32. Elsebaay, A., Adma, M., Ramadan, M.: Analyzing the effect of ambient temperature and loads power factor on electric generator power rating . World Acad. Sci. Eng. Technol. Int. J. Energy Power Eng. 11(2), 171–176 (2017)
33. Mohanan, V.T.: Thermal modelling of permanent magnet machines using double layer winding. Master thesis (2016)
34. Badran, O., Sarhan, H., Alomour, B.: Thermal performance analysis of induction motor. Int. J. Heat Technol. 30(1), 75–88 (2012)
35. Anatychuk, L.I., Luste, O.J.: On the reliability of thermoelectric cooling and generator modules. In: 17th Intemational Conference on Thermoelectric, Japan, Nagoya (1998)
36. Liu, M., et al.: Reliability evaluation of a tidal power generation system considering tidal current speeds. IEEE Trans. Power Syst. 31(4), 3179–3188 (2015)
37. Power Transformer—Part7: Loading Guide for Oil-Immersed Power Transformers. IEC Std. 60076–7 (2005)
38. El-Faraskoury, A., Ghoneim, S., Alaboudy, A.K., Salem, R., Ward, S.A.: Practical and theoretical investigation of current carrying capacity (ampacity) of underground cables. Adv. Elect. Eng. Syst. 1(3), 163–169 (2012)
39. Song, S., et al.: The effect of biofouling on the tidal turbine performance. In: Applied Energy Symposium (2019)
40. Abunima, H., The, J.: Reliability modeling of PV systems based on time-varying failure rates. IEEE Access 8, 14367–14376 (2020)
41. https://www.siemensgamesa.com/en-int
42. https://www.seagen.com
43. https://tidesandcurrents.noaa.gov
44. Jardini, J., et al.: Daily load profiles for residential, commercial and industrial low voltage consumers. IEEE Trans. Power Delivery 15(1), 375–380 (2000)

How to cite this article: Nargeszar, A., Ghaedi, A., Nafar, M., Simab, M.: Reliability evaluation of the renewable energy-based microgrids considering resource variation. IET Renew. Power Gener. 17, 507–527 (2023). https://doi.org/10.1049/rpg2.12611